Chapter 3

Properties of LDH/polymer micro- and nanocomposites

Carbonate- and stearate-intercalated layered double hydroxides were used as fillers to prepare polymer micro- and nanocomposites respectively. The stearate-modified LDH starting material was a bilayer intercalated clay. During melt compounding, excess stearates were released and the clay reverted to a monolayer-intercalated form. The exuded stearate acted as a lubricant, lowering the melt viscosity of the poly(ethylene-co-vinyl acetate) and linear low-density polyethylene matrices. Strong hydrogen bond interactions between the chains of poly(ethylene-co-vinyl alcohol) and the clay platelet surfaces overwhelmed the lubrication effect and caused an increase in the melt viscosity of this matrix. The notched Charpy impact strength of this composite was almost double that of the neat polymer. It appears that this can be attributed to the ability of the highly dispersed and randomly oriented nanosized clay platelets to promote extensive internal microcavitation during impact loading. The creation of a large internal surface area provided the requisite energy-dissipation mechanism.

3 PROPERTIES OF LDH/POLYMER AND NANOCOMPOSITES

3.1 POLYMER COMPOSITES

Polymer composites have attracted attention due to their unique structure and enhanced properties. IUPAC defines a composite as "a multicomponent material comprising multiple different (non-gaseous) phase domains in which at least one type of phase is a continuous phase" according to specifications (Work *et al.*, 2004). A nanocomposite refers to every type of composite materials having one of the components in the nanometre size range at least in one dimension. Manias *et al.,* (2007) defined a nanocomposite as a "fundamentally new material (hybrid) in which the nanometre scale component/structure gives rise to intrinsically new properties not present in the respective macroscopic composites or pure components". New properties are envisaged to originate from the interaction of the polymer and filler at the interface. A polymer composite is made of three constituents, i.e. the matrix, the filler (LDH in this study) and the interfacial region. The interfacial region is a 'communication bridge' between the filler and matrix and is conventionally ascribed properties different from those of the bulk matrix because of its proximity to the surface of the filler (Vaia & Wagner, 2004). These authors further expound it in terms of the radius of gyration of the matrix (*R*g), which is the key spatial parameter to which the majority of the polymer's static and dynamic properties can be ultimately related and has a value in a few tens of nanometres. How then do nanocomposites differ from conventional composites? Vaia and Wagner (2004) cited six interrelated distinguishing qualities of polymer nanocomposites:

- Low percolation threshold (~0.1–2 vol %)
- Particle-particle correlation (orientation and position) arising at low volume fraction ($\phi_c < 0.001$)
- Large number density of particles per particle volume (10^6–10^8 particles/μm^3)
- Extensive interfacial area per volume of particles (10^3–10^4 m^2/mL)
- Short distances between particles (10–50 nm at ϕ ~ 1–8 vol %)
- Comparable size scales among the rigid nanoparticle inclusions, distance between particles and the relaxation volume of polymer chains.

Due to the small aspect ratio of spherical particles, the first two points do not apply to them.

Additive/filler materials are used to reduce costs or enhance properties such as tensile strength and modulus of polymer matrices (Hancock, 1995). Different types of filler are used to obtain polymer nanocomposites based on dimensionality/geometry. These include zero-dimensional nanoparticles (inorganic nanoparticles), one-dimensional nanoparticles (carbon nanotubes), two-dimensional nanoparticles (clays and LDHs), and three-dimensional nanoparticles (polyhedral oligomeric silsesquioxanes). The filler employed in this study falls under the two-dimensional category. Table 3.1 is a summary of other nanostructured layered materials that can be used as additives in polymer matrices. The two-dimensional platelet fillers lead to a lamellar microstructure. Hence the polymer composites have found application for their barrier properties such as reduced gas and vapour permeability. Depending on the aspect ratio of the platelets, they may be used to improve mechanical properties.

Table 3.1. Layered nanostructured materials for potential use in polymer composites (Adapted from Utracki *et al.*, 2007)

Clay type	**Examples**
Phyllosilicates	Montmorillonite (MMT), bentonite (BT), hectorite, talc, vermiculite, micas, illite, attapulgite, etc.
Layered silicic acid	Kanemite, layered organosilicates
Mineral layered hydroxides	Brucite [$Mg(OH)_2$], gibbsite [$Al(OH)_3$]
Layered double hydroxides (LDHs)	$[M^{2+}_{(1-x)}M^{3+}_{x}(OH)_2]^{Y+}(A^{n-Y/2})\ mH_2O$, e.g. $Mg_6Al_{3.6}(OH)_{18.8}(CO_3)_{1.7}H_2O$
Layered aluminophosphates	Berlinite (AlPO), vantasselite [$Al_4(PO_4)_3(OH)_3{\cdot}9H_2O$]
M^{4+} phosphates and phosphonates	M^{4+}= Ti, Zr, or Sn, e.g. α–form: $Zr(HPO_4).2H_2O$
Chlorides	$FeCl_3$, FeOCl, CdI_2, $CdCl_2$
Chalcogenides	TiS_2, $(PbS)_{1.18}(TiS_2)_2$, MoS_3
Cyanides	$Ni(CN)_2$
Oxides	$H_2Si_2O_5$, graphite oxide, V_6O_{13}, $HTiNbO_5$
Others	Graphite, boron nitride

The pioneering work done by Toyota into clay-based polymer nanocomposites increased interest and research into clay-based polymer composites, dating back to 1986 (Kawasumi,

2004). Research has focused mostly on smectite-based polymer composites. Anionic clays such as layered double hydroxides (LDHs) are a potential alternative for the preparation of polymer composites. This can be achieved since LDHs possess a layered structure similar to that of layered silicates or cationic clays. It is well established that the dispersion of particles with high aspect ratios, e.g. fibres and platelets, in polymeric matrices improves the mechanical properties. However, good interfacial adhesion and a homogeneous dispersion are prerequisites (Pradhan *et al.*, 2008). Nanostructured clays can improve a wide range of polymer properties and are therefore ideal for polymer-clay nanocomposite preparations. The resulting polymeric hybrids exhibit improved gas barrier properties, mechanical properties (Hsuesh & Chen, 2003; Wang *et al.*, 2006), enhanced flame retardancy (Zammarano *et al.*, 2005; Costa *et al.*, 2005; Chen & Qu, 2003 & 2004; Zubitur *et al.*, 2009), UV and photo-stability (Bocchini *et al.*, 2008) or ease of photo prodegradability (Magagula *et al.*, 2009), etc.

3.2 POLYMER COMPOSITE STRUCTURES

Organoclay dispersion within a polymer matrix gives rise to three possible structures, i.e. phase separated, intercalated and/or delaminated/exfoliated composites, as shown in Figure 3.1. These structures are usually probed by two complementary techniques, namely X-ray diffraction (XRD) and transmission electron microscopy (TEM). The former gives the degree of separation and the latter serves as a visual confirmation of the XRD analysis.

3.2.1 Phase separated composites

Phase separation results from the polymer chains failing to penetrate the interlayer space of the layered material. The composite retains the same properties as conventional microcomposites. Hence the d-spacing remains the same as that of the clay.

3.2.2 Intercalated composites

In these composites the polymer chain(s) is intercalated within the interlayer of the LDH. They normally exhibit a well-ordered morphology with alternating inorganic and polymeric layers or periodically stacked layers. The composite is made of alternating polymer and inorganic layers. The resulting clay-polymer hybrid exhibits increased d-spacing.

3.2.3 Exfoliation/delamination composites

This structure describes a case where the LDH layers are completely and uniformly dispersed in a polymer matrix. It is identified by the absence of diffraction peaks or basal reflection. This observation is thought to be due to a large increase in the layer separation > 8 nm or lack of ordering or registry (Alexandre & Dubois, 2000). In some instances intercalated and exfoliated structures may co-exist; this is illustrated by the broadening of primary diffraction peaks. To eliminate ambiguous conclusions, TEM is normally used to confirm the results obtained from XRD. Some studies report the exfoliation of surfactant-intercalated LDHs (Leroux *et al.*, 2001; Khan and O'Hare, 2002; Fischer, 2003). In general, a higher degree of exfoliation/dispersion of LDHs has been observed in polar rather than in non-polar matrices. The preparation of polymer composites from polyolefins is difficult due to their low polarity. Hence they do not interact effectively with the LDHs. Dispersion of LDHs in non-polar matrices through melt compounding has been explored using maleic anhydride grafted polyethylene (PE-g-MA) as a compatibiliser (Costa *et al.*, 2005). It is important to note that full exfoliation and full intercalation are seldom observed in nanocomposites.

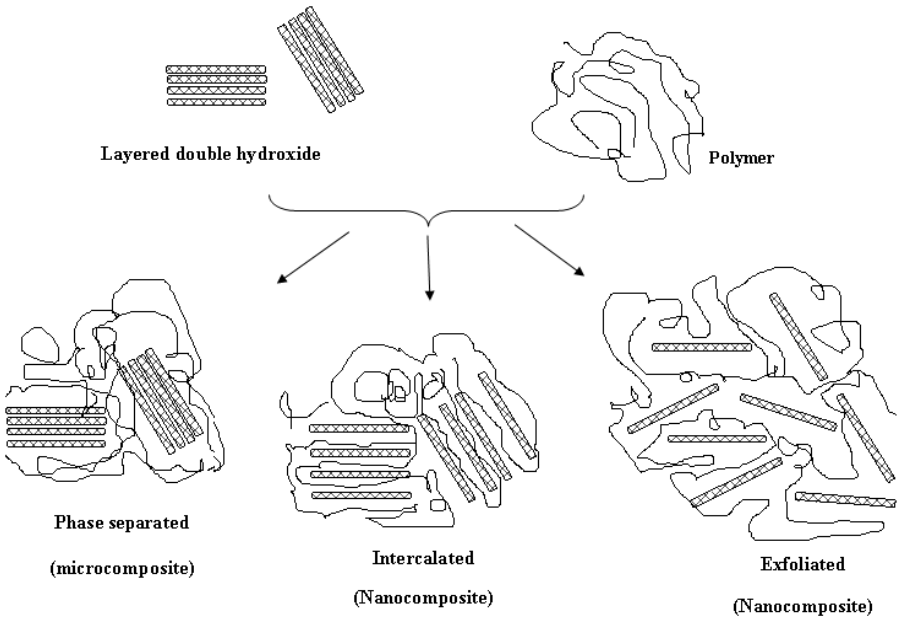

Figure 3.1. Polymer composite structures

The structures that arise are related to the types of interfacial interaction that are favoured between the polymer and the clay. Vaia and Giannelis (1997) proposed three main clay-polymer interactions: polymer-surface, polymer-surfactant and surfactant-surface. They concluded that to achieve complete clay sheet dispersion, a very favourable polymer-surface interaction was necessary (Vaia and Giannelis 1997; Fischer 2003). Therefore the properties displayed by the polymer composite result from these associations.

3.3 LDH-BASED POLYMER COMPOSITE PREPARATION

Polymer-clay composites are mainly prepared in three ways, namely in situ polymerisation (Moujahid *et al.*, 2002; Lee & Im, 2007; Huang *et al.*, 2011), solution-intercalation methods (Ramaraj *et al.*, 2010) and melt-processing (Zammarano *et al.*, 2006).

3.3.1 In situ polymerisation

This is the first and most widely used mode of preparation of clay-based nanocomposites. It has been adopted for the preparation of LDH-based nanocomposites. It combines the basic principles of intercalation of LDHs, namely co-precipitation, regeneration and intercalation via organic/inorganic pillared LDHs (ion exchange), as shown in Figure 3.2. In the case of pillared LDHs, the pillaring agent is chemically active and hence interacts with the polymer chain (Hseuh & Chen, 2003). Usually, the first step entails the intercalation of the monomers/ionomers into the LDH. Polymerisation is initiated by thermal or radiation treatment and is also facilitated by organic initiator and catalyst (Whilton *et al.*, 1997). Recently, polymerisation has been reported to be initiated by microwave irradiation (Herreo *et al.*, 2011). This type of polymerisation makes thermosetting polymer-nanocomposites possible, e.g. epoxy-organoclay nanocomposites.

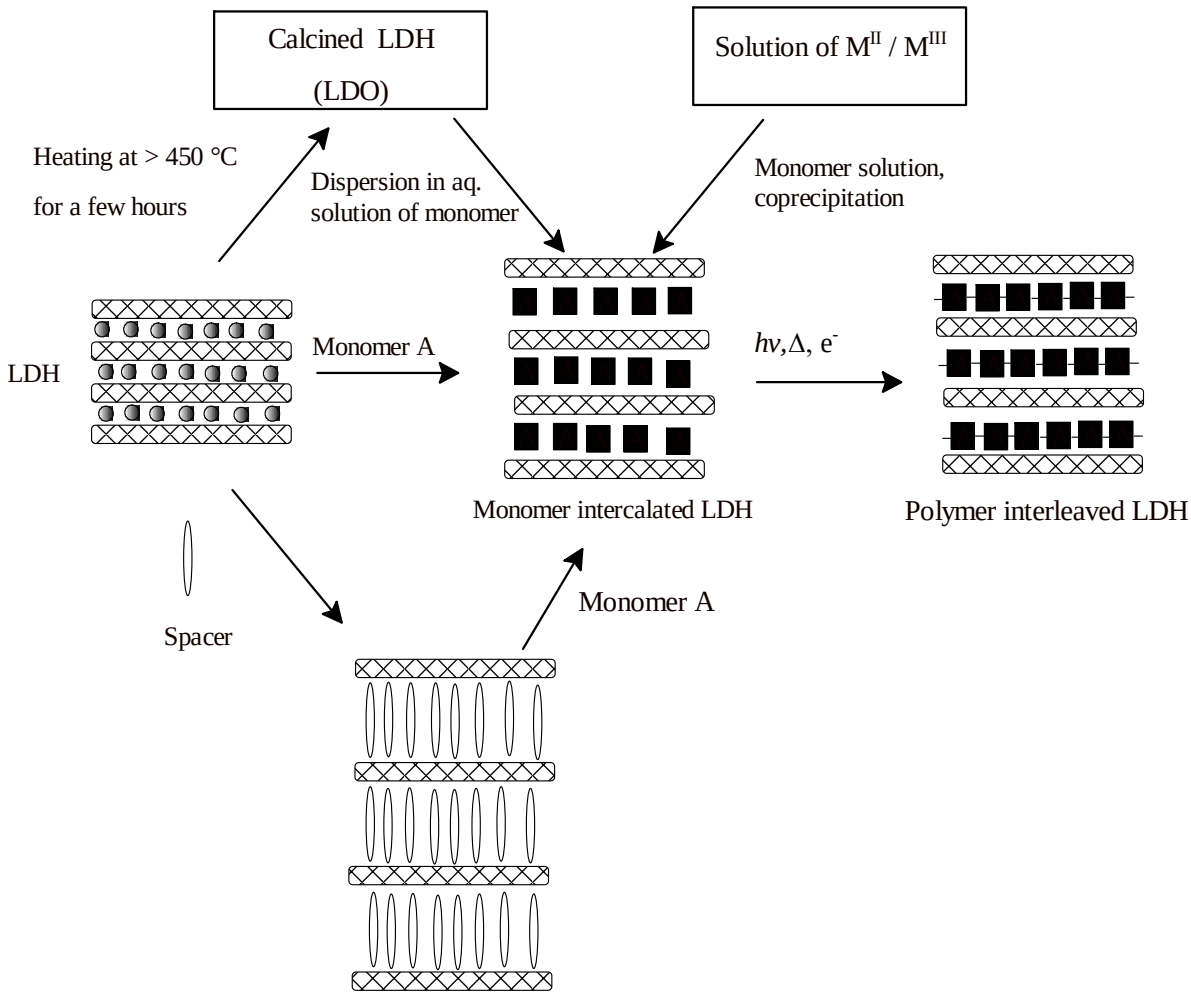

Figure 3.2. Schematic pathways of in situ polymerisation within the LDH layers in the preparation of polymer/LDH nanocomposites (Adapted from Costa *et al.*, 2008)

However, in-situ polymerisation has two limitations. Firstly, there is the distance between the monomers when they are strongly anchored to the host matrix. Secondly, there is the condition that when polymerisation takes place (temperature, pH or redox reaction), it must leave the layered structure intact. This method has been employed with success in the preparation of the LDH-based nanocomposites listed in Table 3.2.

Table 3.2. Summary of in situ polymerisation in LDH-based nanocomposites

LDH	Monomer	Conditions	Reference
Mg-Al	Dimethyl terephthalate	Ethylene glycol catalyst	Cui *et al.*, 2012
Li-Al	Amino benzoic acid (different isomers)	Ion exchange	Isupov *et al.*, 2001
Zn-Al	Vinyl benzene sulphonate	Co-precipitation	Moujahid *et al.*, 2003
Mg-Al	Aspartate	Co-precipitation	Whilton *et al.*, 1997
Ca-Al	Styrene-4-sulphonate	Co-precipitation	Vieille *et al.*, 2004
Zn-Al	Styrene sulphonate	Co-precipitation	Vieille *et al.*, 2004
Mg-Al	Methyl methacrylate (MMA)	Via 10-undecenoate pillared LDH. Catalyst (2,2′-azobisisobutyronitrile) used to prepolymerise MMA	Wang *et al.*, 2005
Cu-Cr Cu-Al	Analine	Via terephthalate or hexacyanoferate pillared LDH	Challier & Slade, 1994
Mg-Al	Acrylate	Via dodecylsulphate pillared LDH	O'Leary *et al.*, 2002

3.3.2 Solution intercalation

Solution intercalation is also referred to as solution blending and solution casting. This particular method entails the solubilisation of the polymer resin in an organic solvent. The solvents employed include toluene, chloroform, acetonitrile, xylene and dimethylacetamide. The mixed metal aqueous salts may be precipitated into the former solution. In other cases organo-modified LDHs are added to the polymer solution. Chen *et al.* (2003, 2004) synthesised the same polymer composite using the solution intercalation synthesis method. The organo-LDH was added to a solution of PE-g-MA in xylene and the mixture was refluxed in nitrogen for 24 h. The polymers used in this method are normally water soluble, such as PEO, poly(vinyl alcohol) and poly(vinyl pyrrolidone). Table 3.3 provides a summary of a few selected solution intercalation formulations.

Table 3.3. Summary of solution intercalation in LDH-based nanocomposites

LDH	Polymer	Solvent	Reference
Mg-Al	PE-g-MA	Xylene	Chen *et al.*, 2003
Zn-Al	LLDPE	Xylene	Chen *et al.*, 2004
Mg-Al	Poly(styrene-co-methylstyrene) grafted polyaniline	Xylene	Abbasian, 2011
Zn-Al	PVA	Water	Marangoni *et al.*, 2010
Mg-Al	Silicone rubber	Chloroform	Pradhan *et al.*, 2010
Mg-Al	PVA	Water	Ramaraj *et al.*, 2010
Mg-Al	Polyurethane	Tetrahydrofuran (THF)	Kotal *et al.*, 2009
Mg-Al	Poly(propylene carbonate)	Cyclohexanone	Du *et al.*, 2006
Mg-Al	Poly(vinyl chloride)	THF	Liu *et al.*, 2008
Mg-Al	Ethylene vinyl acetate	Toluene	Kuila *et al.*, 2007
Mg-Al	Ethylene propylene diene terpolymer	Toluene	Achyra *et al.*, 2007

However, the use of organic solvents makes the method environmentally unfriendly and they are not easily removed. In some cases small solvent particles intercalate into the clay gallery rather than the polymer.

3.3.3 Melt processing

This method has been considered to be most challenging, yet it can be easily adopted for industrial product manufacture. It involves the incorporation of the filler into a molten polymer through extrusion, kneading and, to a lesser extent, injection moulding (Manias *et al.*, 2007). In addition to the thermodynamic driving force for filler dispersion, mechanical shear has kinetic contributions. A high degree of dispersion is obtained, depending on the processing conditions and the polarity/affinity of the polymer to the organoclay. Good exfoliated structures have been reported as a result of adequate mean residence time, viscosity of the matrix and shear rate (Cho & Paul, 2001). This method is environmentally friendly and economically advantageous due to the absence of solvents and is a cost-

effective way to prepare samples in large quantities. It has been successfully employed by the researchers cited in Table 3.4.

Table 3.4. Summary of melt-processing examples in LDH based nanocomposites

LDH	Organic modifier	Polymer	Reference
Mg-Al	Dodecylbenzene sulphonate (DBS) 4-hydroxybenzene sulphonate (HBS	Poly(p-dioxanone)	Zubitur *et al.*, 2009
Mg-Al	Lauric acid	Poly(L-lactic acid)	Katyar *et al.*, 2011
Mg-Al	Dodecyl sulphate	LLDPE	Costa *et al.*, 2007
Mg-Al	Dodecyl sulphate Dodecyl benzene sulphonate Octyl sulphate	PET	Lee *et al.*, 2006
Zn-Al	Dodecyl sulphate	Polylactic acid	Wang *et al.*, 2010
Mg/Al	Stearic acid	Poly(vinyl) chloride	Chen, 2007
Mg-Al	Dodecyl benzene sulphonate	Polypropylene	Wang *et al.*, 2011
Mg-Al	Dodecyl benzene sulphonate	Polypropylene	Coiai *et al.*, 2010
Mg-Al	2-ethyhexyl sulphate Dodecyl sulphate Eicosyl sulphate	LDPE	Muksing *et al.*, 2011
Mg-Al	Dodecyl sulphate	Nylon 6 (polycaprolactam)	Du *et al.*, 2007
Mg-Al	Dodecyl sulphate	Polypropylene	Lonkar *et al.*, 2009

In the non-polar matrices, such as polyethylene and polypropylene matrices, compatibilisers such as polyethylene grafted maleic anhydride (PE-g-MA) are used to improve the compatibility between the clay and the polymer.

Other methods used in the preparation of polymer nanocomposites, though used to a lesser extent, include co-vulcanisation (Okada & Usuki, 1995), solid state intercalation (Gao *et al.*,

2001) and sol-gel methods (Carrado & Xu, 1999). Vaysse *et al.* (2003) combined chimie douche and redox exchange for the preparation of monomeric intercalated LDH, followed by its in situ polymerisation, resulting in a polyacrylate-intercalated composite.

3.4 PROPERTIES OF LDH-BASED POLYMER NANOCOMPOSITES

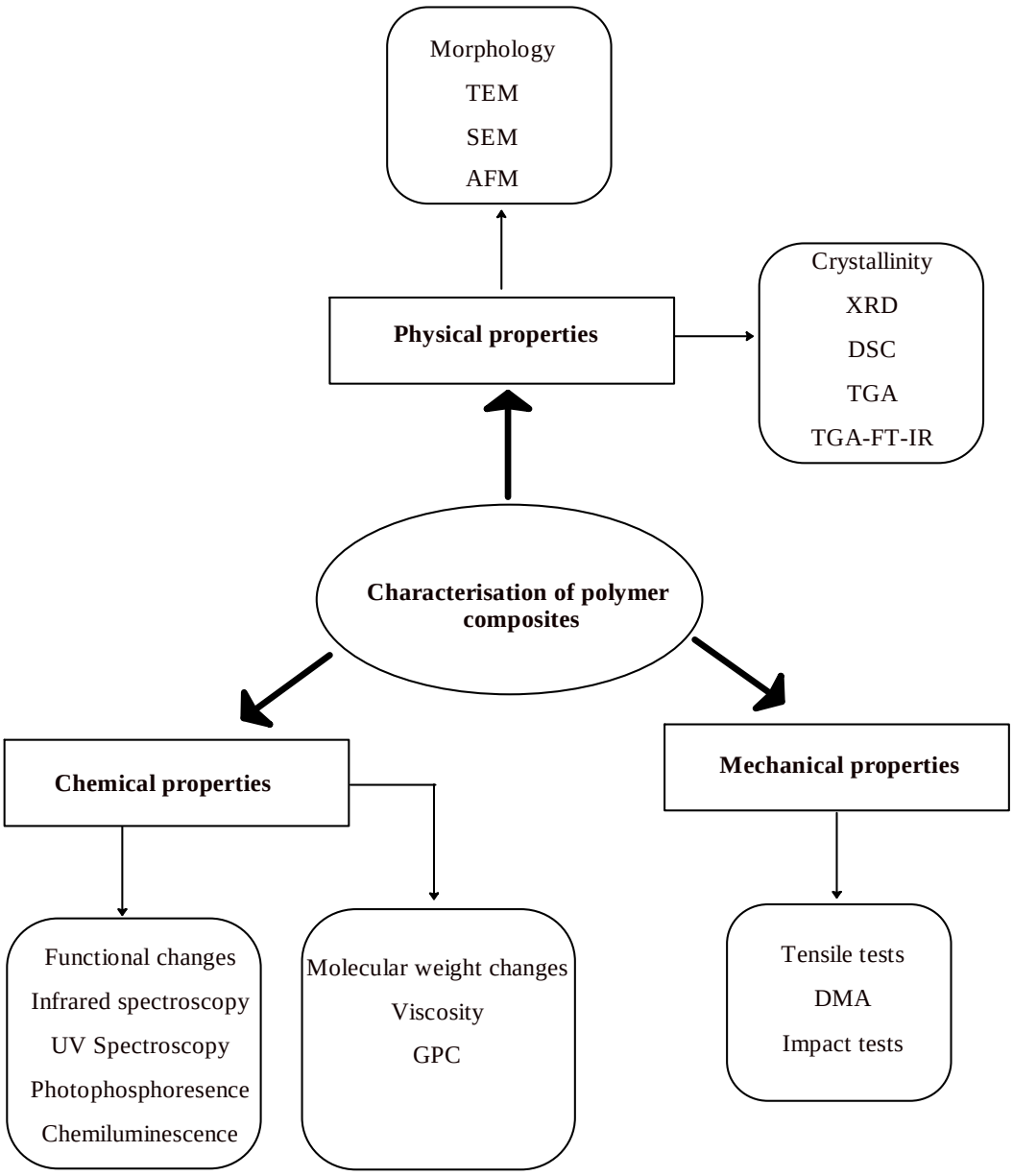

Figure 3.3. Characterisation of LDH-based polymer composites

Figure 3.3 shows a wide variety of characterisation techniques available for the analysis of the properties of polymer nanocomposites. These include X-ray diffraction (XRD), transmission electron microscopy (TEM), scanning electron microscopy (SEM), atomic force microscopy (AFM), thermogravimetric analysis (TGA). Mechanical properties are probed by tensile testing, impact testing and dynamic mechanical analysis (DMA). Chemical changes in the polymer composite matrix are examined through rheology, infrared and UV spectroscopy, gel permeation chromatography, etc. The properties discussed in the following sections are those that were also investigated in this study.

3.4.1 Physical properties

3.4.1.1 Morphology

Among the previously mentioned characterisation techniques, XRD and TEM are the most frequently used for the determination of the composite structure and degree of dispersion. The increase in the d-spacing has been explained as an indication of successful intercalation of the polymer, whereas its loss is evidence of an exfoliated structure. In this context, most researchers publish work on LDH-based nanocomposites as either intercalated or exfoliated. However, the loss of the primary reflection can be easily misinterpreted as exfoliation yet technical errors, such as a low starting angle, misalignment of sample holder, wrong slit setting or orientation, or the resolution limitations of XRD apparatus (i.e. $2\theta < 2$), will give similar results (Chen & Qu, 2004). In other cases, the disappearance of the primary peak could also be a result of a very low filler loading and crystal defects caused by processing. TEM allows a qualitative understanding of the internal structure and the spatial distribution of various phases, and direct visualisation of the defect structure (Ray & Okamoto, 2003).

Compatibility studies of LDHs with polypropylene (PP), polystyrene (PS), polyethylene (PE) and poly(methyl-methacrylate) (PMMA) were carried out by Nyambo *et al.* (2009.) Good dispersion and nanocomposite formation was obtained from the LDH/PMMA composite. Complete exfoliation in polystyrene/ZnAl LDH composite (derived from solution intercalation) was achieved by decreasing the LDH content, extending the reflux time and employing rapid precipitation (Qui *et al.*, 2005). It is clear from the above that the success of preparing a well-dispersed polymer composite depends on the polarity of the polymer and the chemistry of the filler. In the preparation of LDH-based nanocomposites in

non-polar matrices, maleic anhydride grafted polyethylene is normally employed to improve the compatibility of the LDH with the matrix (Costa *et al.*, 2006).

3.4.1.2 Thermal behaviour

LDH-based polymer composites have been studied particularly for improving the thermal stability of the matrix. The mechanism by which LDHs achieve this is in the same manner as traditional metal hydroxide fillers. LDHs contain bound water, interlayer free water and OH-groups on the metal hydroxide lattice. The decomposition of LDHs is endothermic and releases water vapour, which reduces the amount of combustible volatiles at the surface of the polymer (Costa *et al.*, 2007). The incorporation of LDHs improved the thermal stability of the polymer, but the degradation mechanism remained the same (Zubitur *et al.*, 2009; Liu *et al.*, 2009; Nyambo *et al.*, 2008). Low LDH loading also gave improved thermal stability; this is explained by the nanoscale dispersion. Other factors that affect thermal stability include the intrinsic thermal resistance of the polymer matrix, the nanofiller content, the chemical constitution of the organic modifier, the chemical character of the polar compatibiliser, and lastly access of oxygen to composite material during heating. However, the thermal stability of LDH-based nanocomposites was not improved in all cases. Chiang and co-workers (2011) found deterioration of the thermal stability of poly(L-lactide) (PLLA)/layered double hydroxide composites. They attributed this anomaly to the LDH derivative used (P-LDH) which was considered to accelerate thermal decomposition of the polymer. Thermal behaviour is particularly linked with flame retardation studies in LDH-based polymer composites. A number of researchers have embarked on research into the flame-retardant properties of LDHs in their polymer composites (Costache and Wang, 2006; Jaio *et al.*, 2006; Nyambo *et al.*, 2008). This is important since most flame retardants are halogen-based and these tend to be corrosive and toxic. Hence LDHs are more environmentally friendly alternatives.

Thermal behaviour may also be studied by DSC to follow changes in the melting and crystallisation in the composite matrix. The technique measures temperatures and heatflows associated with transitions in the materials as a function of time and temperature in a controlled atmosphere. The fundamental equation for DSC heatflow is give below, under the assumption that work and mass loss are equal to zero:

$$\Delta H = C_p \Delta T \quad [3]$$

In differential form it is represented as:

$$\frac{dH}{dt} = C_p \frac{dT}{dt} \quad [4]$$

where;

$Cp = specific\ heat\ capacity\ (J/g°C)$

$T = temperature\ (°C)$

$H = heat\ (J)$

$\frac{dH}{dt} = heat\ flow\ (J/min)$

$\frac{dT}{dt} = heating\ rate\ (°C/min$

Crystallinity is calculated as:

$$C = \Delta H / \Delta H100\% * 100\% \quad [5]$$

where

$C = crystallinity\ (\%)$

$\Delta H = heat\ of\ fusion\ (J/g)$

$\Delta H100\% = heat\ of\ fusion\ of\ 100\%\ crystalline\ polymer$

The crystallisation of a polymer is governed by polymer molecules having adequate regular structure and mobility; the temperature should be $T_g < T < T_m$, presence of a nuclei and the rate of crystallisation to be sufficiently high (Utracki 2004). Crystallisation is either homogeneous or heterogeneous; the former occurs when the polymer molecules self-assemble into an ordered state, while in the latter molecules assemble on the surface of a foreign body. In the case of LDH-based composites, LDHs act as heterogeneous nucleation sites. The crystallisation behaviour of LDH-based polymer composites was studied by Ramaraj *et al.* (2010). The LDH particles were found to have a nucleating effect in the polymer matrix.

3.4.2 Mechanical properties

Mechanical properties are investigated by tensile and impact testing, and by dynamic mechanical analysis. The reinforcing property of organoclay in polymer composites depends on the aspect ratio of the fillers, the particle size and distribution, its degree of dispersion and orientation in the matrix, the porosity of the composite and the adhesion at the filler-matrix interface (Cho & Paul 2001; Verbeek & Focke, 2002). The micromechanics of tensile testing of laminated composite materials are represented in a simple mathematical model in which the tensile modulus is described in terms of isostrain and isostress, as illustrated in Figure 3.4. The elastic properties of the composite depend on the orientation of the filler to the applied stress. The effective moduli when the layers are in parallel or in series yield the Voight and Ruess moduli respectively (Ward & Hadley, 1993).

An isostrain condition applies when the strain is the same in all composite layers. Hence maximum stiffness is achieved when the stress is applied parallel to the layers. An isostress condition applies when the layers are orientated transverse to the applied stress and each layer is subjected to the same force. This is under the assumption that the area remains constant through the stack and the stress is the same in all the layers. The effective Young's moduli are given by the equations below (Verbeek & Focke, 2002):

$$Isostrain: E_c = E_m \nu_f + E_p \nu_p \quad [6]$$

$$Isostress: {}^{1}/_{E_c} = {}^{\nu_f}/_{E_m} + {}^{\nu_p}/_{E_p} \quad [7]$$

where

E_c = the tensile modulus of the composite

E_{p} = the tensile modulus of the polymer

E_{m} = tensile modulus of the filler

ν_p and ν_f = volume fraction associated with zero porosity of the polymer and filler respectively.

The particles are assumed to adhere perfectly to the matrix. Several empirical modifications to the model have been made by Nicolais & Narkis; Kerner, Faber & Farris; and Nielson, Haplin-Tsai to mention a few (cited in Utracki, 2004).

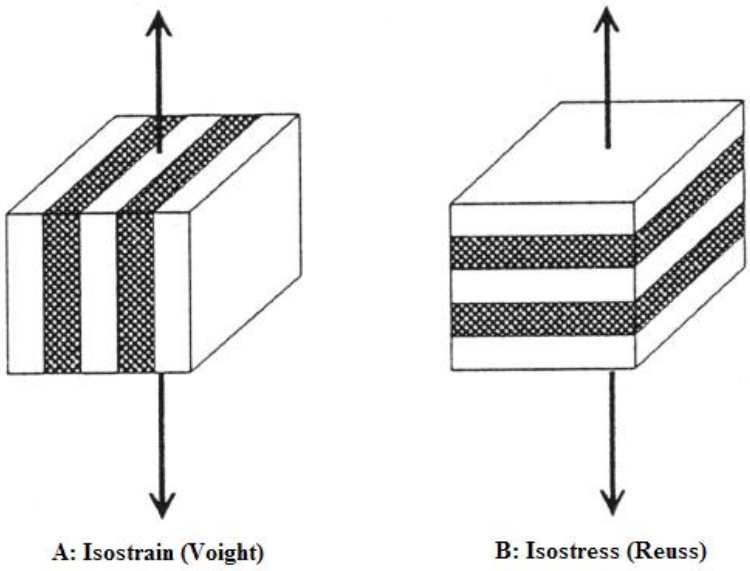

Figure 3.4. Mixing rule conditions for layered composites (Adapted from Verbeek & Focke, 2002)

Camino *et al.* (2001) found that tensile tests indicate that as far as the elongation to break and ultimate strength are concerned, the LDH system behaves similarly to other fillers. Lonkar *et al.* (2012) prepared PP/LDH nanocomposites using PP-g-MAH as a compatibiliser. The specimens showed an increase in modulus and tensile strength parameters, which is an indication of the reinforcing property of LDHs. However, they found that the impact strength and elongation at break steadily decrease with increase of the organo-LDH content.

The incorporation of fillers in the polymer matrix results in a heterogeneous system. When an external load is applied, these particles act as stress concentrators and the magnitude is dependent on the geometry of the particles (Zuiderduin *et al.*, 2003). Rigid fillers to be used as polymer-toughening agents must meet the following prerequisites as given by Zuiderduin *et al.* (2003):

- The particles should be small in size (less than 5 µm). These provide a stable free volume, whereas larger particles act as initiation sites for fracture.
- The aspect ratio must be close to unity to avoid high stress concentrations.

- The particles must debond prior to the yield strain of the polymer matrix in order to allow the stress state of the matrix material to change.
- The particle must be dispersed homogeneously in the polymer matrix; aggregation should be avoided.

Polymer-toughening modifiers alter the stress state in the material around the particles and induce extensive plastic deformation, e.g. multiple crazing (see Figure 3.5), shear banding (see Figure 3.6), crazing with shear yielding, rubber particle stretching or tearing, and debonding at the inorganic filler particles (Kim *et al.*, 1998). These deformations constitute a range of different energy-absorption mechanisms, hence preventing premature fracture.

Crazes are stabilised stress cracks whose separation surfaces are bridged by stretched fibrils and films (see Figure 3.5). A typical fibril diameter is 0.01–0.1 μm. A craze differs from a crack in that it continues to support a load. Craze propagation absorbs fracture energy and effectively increases the toughness of a polymer. It is typically identified by whitening of the crazed region. The white colour is caused by light scattering. Necking of tensile test specimens is not observed in a crazing scenario. However, it is observed in shear banding. The typical size of a craze is approximately 0.5 μm.

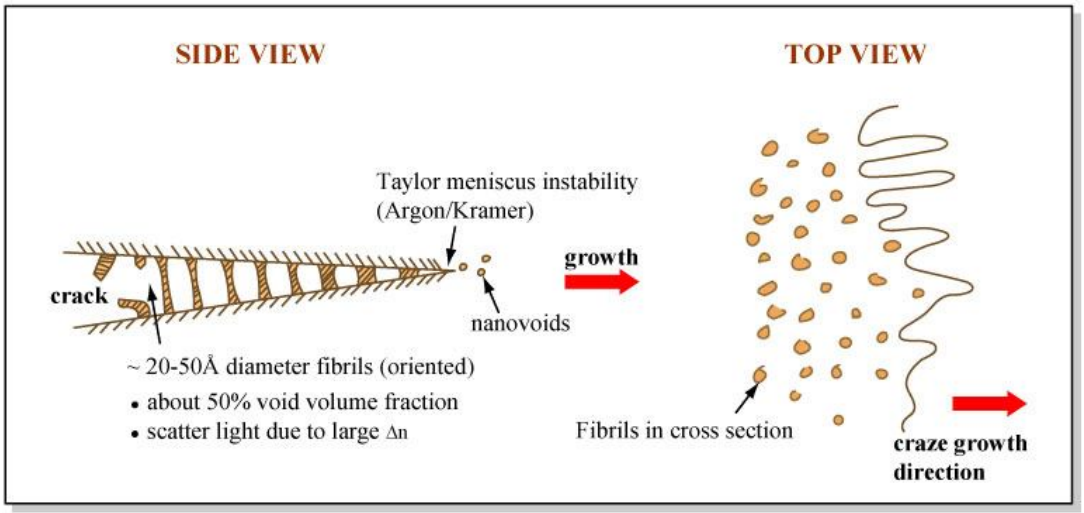

Figure 3.5. Craze yielding (Adapted from MIT Open Course Ware, 2009)

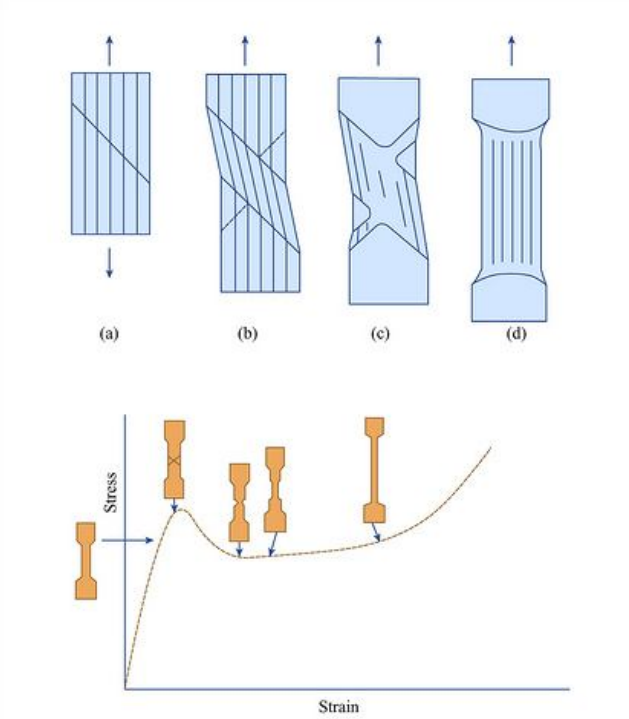

Figure 3.6. Shear banding (Adapted from MIT Open Course Ware, 2009)

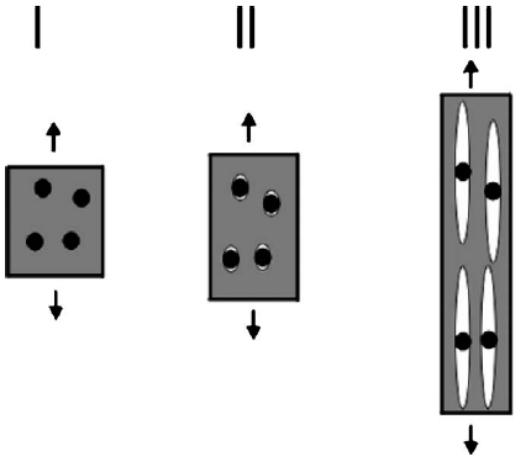

Figure 3.7. Polymer-toughening mechanism with rigid particles (Kim *et al.*, 1998) (Figure adapted from Zuiderduin *et al.*, 2003)

Figure 3.7. shows a polymer-toughening mechanism proposed by Kim *et al.* (1998). The filler is required to debond, hence creating free volume at a sub-micron level, which is a cavitation mechanism similar to that found in rubber-toughened matrices. The figure depicts the following:

I. *Stress concentration* – The modifier act as stress concentrators, because they have different elastic properties from those of the polymer matrix.
II. *Debonding* – Stress concentration gives rise to a build up of triaxial stress around the filler particles and leads to debonding at the particle-polymer interface.
III. *Shear yielding* – The voids caused by debonding alter the stress in the polymer matrix surrounding the voids. This reduces sensitivity towards crazing since volume strain is released. The shear yielding mechanism becomes operative and the material is able to absorb large quantities of energy upon fracture.

Generally, very few works of literature site mechanical property improvement for LDH-based polymer composites (Lonkar *et al.*, 2012).

Various investigations have demonstrated the thermotropic behaviour of the interlayer anions in surfactant-intercalated LDHs (Nhlapo *et al.*, 2008; Focke *et al.*, 2010). Nhlapo *et al.* (2008) showed that fatty acid-intercalated LDH that was beyond the AEC levels appeared to melt partially without reforming, below polymer processing temperature (120 °C). Globular residues were observed, giving a façade of a completely molten LDH-stearate. However, this was attributed to the exuded stearate anions which formed a droplet on the remaining LDH-stearate platelet. The transudation of the interlayer anions in bilayer intercalated LDHs is envisaged to include stages of removal of interlayer water and excess anions, giving a monolayer orientated residue. The study by Nhlapo *et al.* (2008) suggested that the LDH-fatty acid dispersion in polymer matrices would not result in ordinary exfoliation or delamination. It was therefore of interest to explore this anomaly further with regard to the effect of the exuded anions on the matrix and the utility of LDHs as functional fillers. Hence in the present investigation both the unmodified LDH-carbonate (LDH-CO_3) and the modified LDH-stearate (LDH-St) were compounded into polyethylene copolymers of differing polarities.

The polymers of choice were poly(ethylene)-co-vinyl alcohol (EVAL), poly(ethylene)-co-vinyl acetate (EVA) and linear low-density polyethylene (LLDPE). EVAL is widely used in the packaging of foods and non-foods because of its excellent gas- and flavour-barrier properties. EVAL is a crystalline random copolymer of ethylene and vinyl alcohol with the molecular formula represented by the structure (EVAL EUROPE Product Sheet):

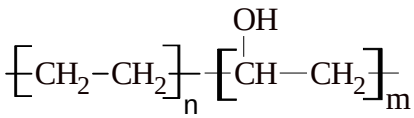

EVAL

EVA is a copolymer of ethylene and vinyl acetate. It has applications in packaging (cling wrap), electrical insulation, hot-melt adhesives, foam rubber and biomedical engineering (drug delivery). Its molecular formula is:

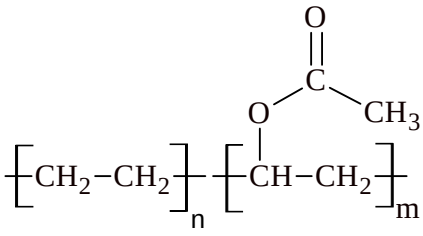

EVA

LLDPE is a copolymer of ethylene which has a short-branched hydrocarbon chain. Like the other polymers used in the study, it finds application mainly in the packaging industry and flexible tubing. Its formula is:

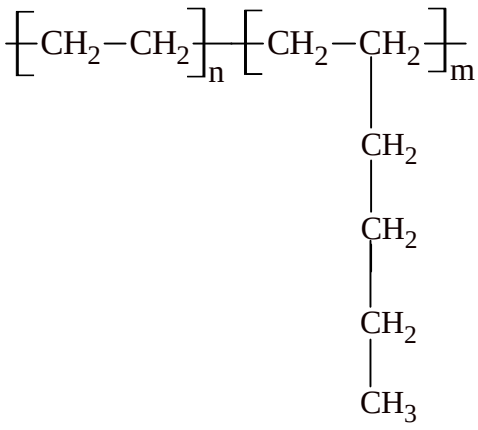

LLDPE

In this study a combination of complementary techniques was employed to investigate the structure-property relationship of the composites obtained there.

3.5 EXPERIMENTAL

3.5.1 Materials

The 1-hexene random copolymer-based linear low density polyethylene (LLDPE) was supplied by Sasol Polymers (South Africa) rotomolding grade HR411 (density 0.939 g cm^{-3}). Poly(ethylene-co-vinyl acetate) (EVA) grade EV101 (density 0.941 g cm^{-3}) containing 18 mol % vinyl acetate was supplied by Asia Polymer Corporation, Taiwan. Poly(ethylene-co-vinyl alcohol) (EVAL) grade T101B (density 1.17 g cm^{-1}) containing 68 mol % vinyl alcohol was obtained from Kuraray, Belgium. The melt flow index (MFI) values measured at 190 °C/2.16 kg in units of g/10 min were 3.5, 1.8 and 1.7 for the LLDPE, EVA and EVAL respectively. The materials required for the modification of LDH have been described in Chapter 2.

3.5.2 Preparation of LDH-stearate

A detailed experimental procedure was described in Section 2.5.2 for the intercalation of stearic acid into LDH. The results of the repeat experiments are shown in Appendix B.

3.5.3 Preparation of polymer/LDH-St

The polymer composites in the study were prepared with both pristine and modified LDHs. The constitutive proportions of the LDHs in the composites prepared were 5 and 10 by wt% of organoclay. The polymer/LDH composites were prepared by the melt-compounding process in a TX28P co-rotating twin screw extruder, with a screw diameter of 28 mm with an L/D ratio of 18. The temperature profile from the feed to the die of the extruder was between 100 and 220 °C. An average screw speed of about 170 rpm was used. The extruded polymer and polymer composite strands were water-cooled as they came out of the die. The extrudents were granulated and left to dry overnight at 60 °C. A portion of each sample was used to injection mould dumbbells for the tensile tests. Injection moulding was carried out on an Engel injection moulding machine. The set temperature for zones 1/2/3 and nozzle were 200/210/220/220 ˚C for LLDPE and EVAL composites and 140/150/160/170 ˚C for the EVA composites respectively.

3.5.4 Characterisation

Imaging of fractured surfaces was carried out in a JEOL 5400 SEM and in a JEOL 5400 SEM. The polymer composite samples were fractured after they had been placed in liquid nitrogen. The composites were mounted on the sample holder and coated five times with gold under argon gas using the SEM autocoating unit E5200 (Polaron equipment Ltd).

The degree of dispersion was studied by use of transmission electron microscopy (TEM). Analysis was carried out on a JEOL 2100F, at an accelerated voltage of 200 kV. The samples were prepared by means of cryo-ultramicrotomy in a Lecia-Riechert Ultracut R with EMFCS cryo-attachment, with a nominal thickness of 90 ± 10 nm, and sliced at -80 °C using a diamond knife. Each section was then mounted on a 300 mesh copper/palladium grid and viewed.

Thermogravimetric analysis (TGA) was conducted on a Mettler Toledo A851 TGA/SDTA machine. A small piece of sample (ca. 10 mg) was placed in 70 µl alumina open pans. The temperature was scanned at 10 °C/min in air in the range from 25 to 800 ^{o}C.

Differential scanning calorimetry (DSC) data were collected from a Mettler Toledo DSC 1 instrument. Approximately 5–10 mg of sample was placed in an aluminium pan. A pin hole was made in the lid. The sample was heated from 0 to 250 °C at a scan rate of 10 °C/min and at a N_2 flow rate of 50 ml/min.

Viscoelastic behaviour was studied with a Perkin Elmer DMA 8000 dynamic mechanical analyser (DMA) using the single cantilever bending mode. The applied frequency was 1 Hz. The temperature was scanned at 2 °C min^{-1} from -20 to 180 °C, -80 to 150 °C and -50 to 80 °C for EVAL, LLDPE and EVA respectively.

Melt flow viscosity was determined with a Göttfert High-Pressure Capillary Rheograph 2000 rheometer. The capillary die had a 180 ° entrance angle, a diameter of 1 mm and a length of 30 mm. Measurements were done at 190 °C with shear rates ranging from 1 to 5 000 s^{-1}.

FTIR spectra were recorded on a Perkin Elmer 100 Spectrophotometer with a MIRacle ATR attachment with diamond Zn/Se plate. A piece of solid sample was pressed onto the Zn/Se plate. The reported spectra were obtained over the range 650–4 000 cm^{-1} and represent an average of 32 scans at a resolution of 2 cm^{-1}.

Phase identification was carried out by X-ray diffraction (XRD) analysis on a PANalytical X-pert Pro powder diffractometer. The instrument features variable divergence and receiving slits and an X'celerator detector using Fe-filtered Co K-α radiation (0.17901 nm). X'Pert High Score Plus software was used for data manipulation.

Tensile testing was carried out on a Lloyds Instruments LRX Plus machine according to ASTM D 638 using Type IV dumbbells. Five specimens were tested for each compound. Charpy impact testing was carried out on a Zwick Impact Tester using the 0.5 J hammer. Tensile impact tests were carried out according to ASTM D1822-06 on Type S and L test specimens.

Polarised optical microscopy (POM) was used to study the crystallisation morphology. The samples were sandwiched between two glass slides and heated on a Linkam THMS hot stage (Linkam Scientific Instruments Ltd) from room temperature to 135 °C for LLDPE and its respective composite at a rate of 10 °C/min, and then held at this temperature for 5 min before being cooled at the same rate to 125.5 °C. They were then held isothermally for 10 min, during which time images were taken using a Carl Zeiss POM.

3.6 RESULTS AND DISCUSSION

The two fillers considered in this study are distinguished by the nature of the external planar surface. The LDH-CO_3 featured sheets with exposed hydroxyl groups. They allow strong hydrogen bonding with the alcohol functional groups present in polar matrices such as EVAL. However, these highly polar surfaces would be incompatible with the non-polar LLDPE matrix. In the case of the LDH-stearate, the particles are at least partially covered by stearate anions (Focke *et al.*, 2010). Such surface modification with aliphatic chains should provide improved compatibility with the aliphatic LLDPE chains. The second consideration is the strength of interactions within the clay interlayers. The high charge density and the hydrophilicity of the layers in LDH-CO_3 encumber delamination or

exfoliation of the clay sheets (Adachi-Pagano *et al.*, 2000; Leroux *et al.*, 2001; Hibino & Jones, 2001). In the LDH-stearate, the fatty acid chain ends in the bilayers interact via weak van der Waals forces only. Hence it is much easier to delaminate and disperse this clay in polymer matrices.

The results described below pertain to the 10 wt.% of each respective composite unless stated otherwise. Detailed results of the 5 wt.% composite are presented in Appendix C.

Figures 3.8, 3.9 and 3.10 are SEM images that show the general morphology and texture of freeze-fractured surfaces. In the EVA/LDH-CO_3 and LLDPE/LDH-CO_3 composite (see Figures 3.8 and 3.10), there is clear phase separation of the clay and the polymer. The LDH-CO_3 particles appear to form agglomerates within the polymer matrix. Poor interfacial adhesion is evident in both the LLDPE composites (Figure 3.10). This is shown by the formation of wells around the filler particles. This is also the case for the EVA/LDH-stearate composite. In all the other samples there was relatively good adhesion between the matrix and the filler, shown by the absence of cavities previously occupied by particles. Some spherical cavities were also seen in all the EVAL samples, including the neat polymer. However, they are attributed to volatilisation of residual water during the moulding process.

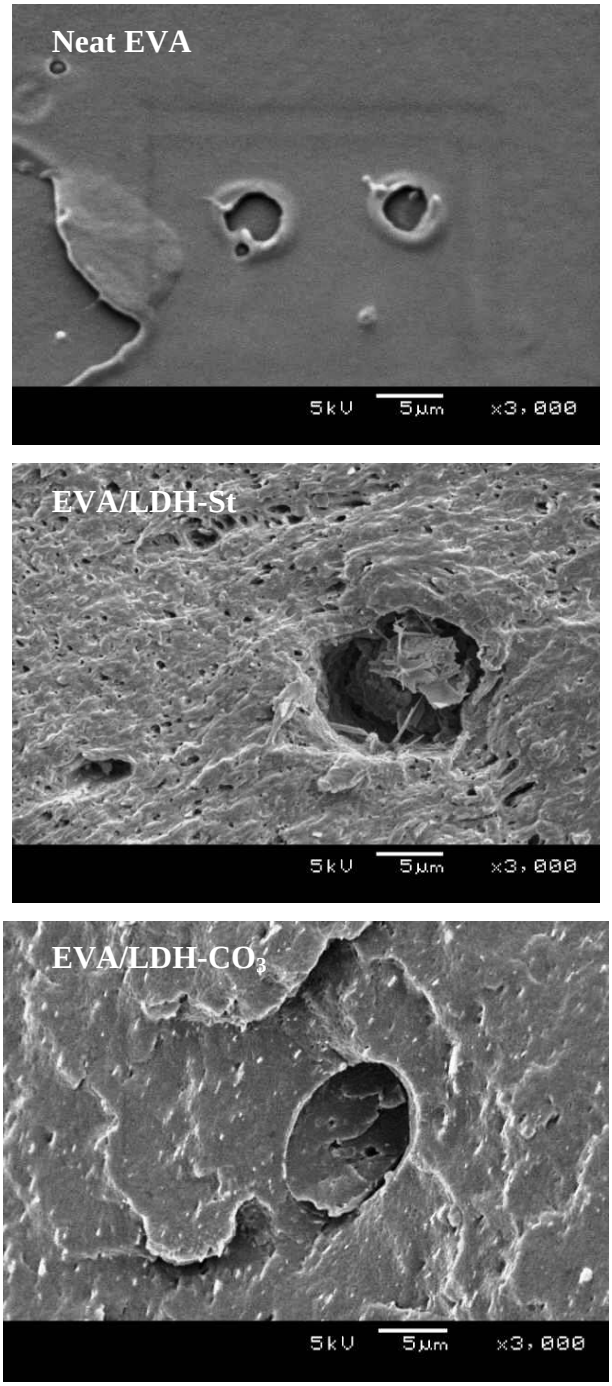

Figure 3.8. Freeze-fractured surface of neat EVA, EVA/LDH-St and EVA/LDH-CO_3. The latter two samples contained 10 wt.% filler.

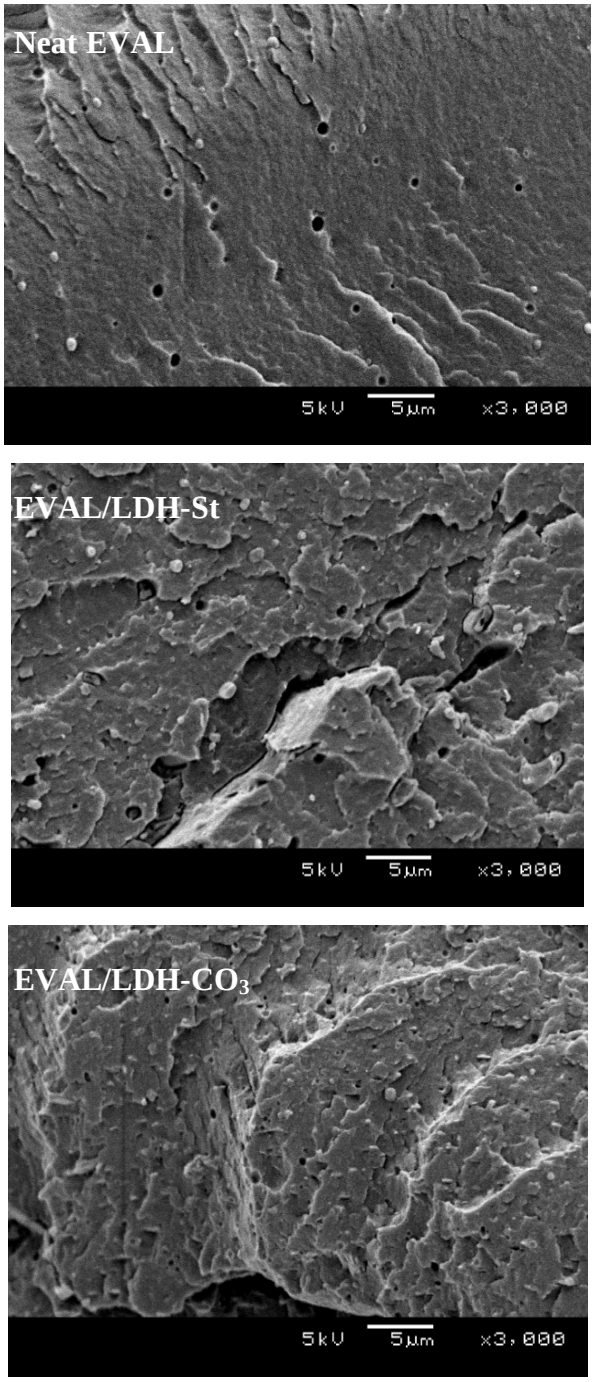

Figure 3.9. Freeze-fractured surface of neat EVAL, EVAL/LDH-St and EVAL/LDH-CO_3. The latter two samples contained 10 wt.% filler.

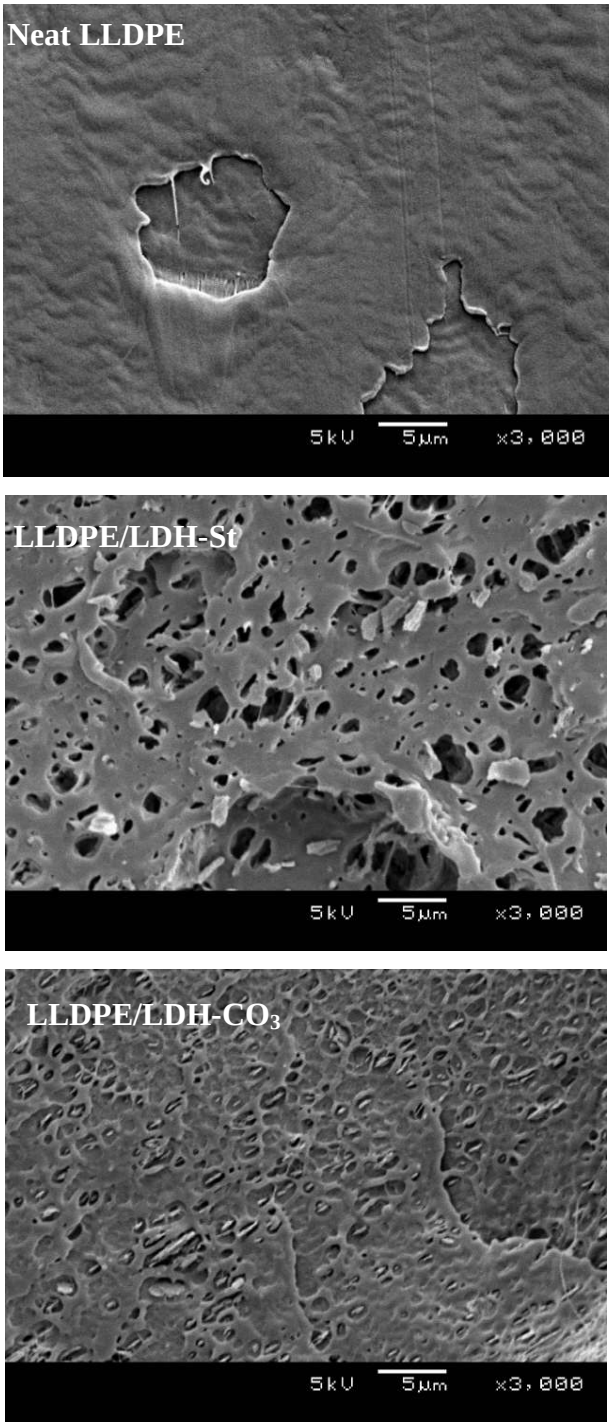

Figure 3.10. Freeze-fractured surface of neat LLDPE, LLDPE/LDH-St and LLDPE LDH-CO_3. The latter two samples contained 10 wt.% filler.

3.6.1 X-ray diffraction

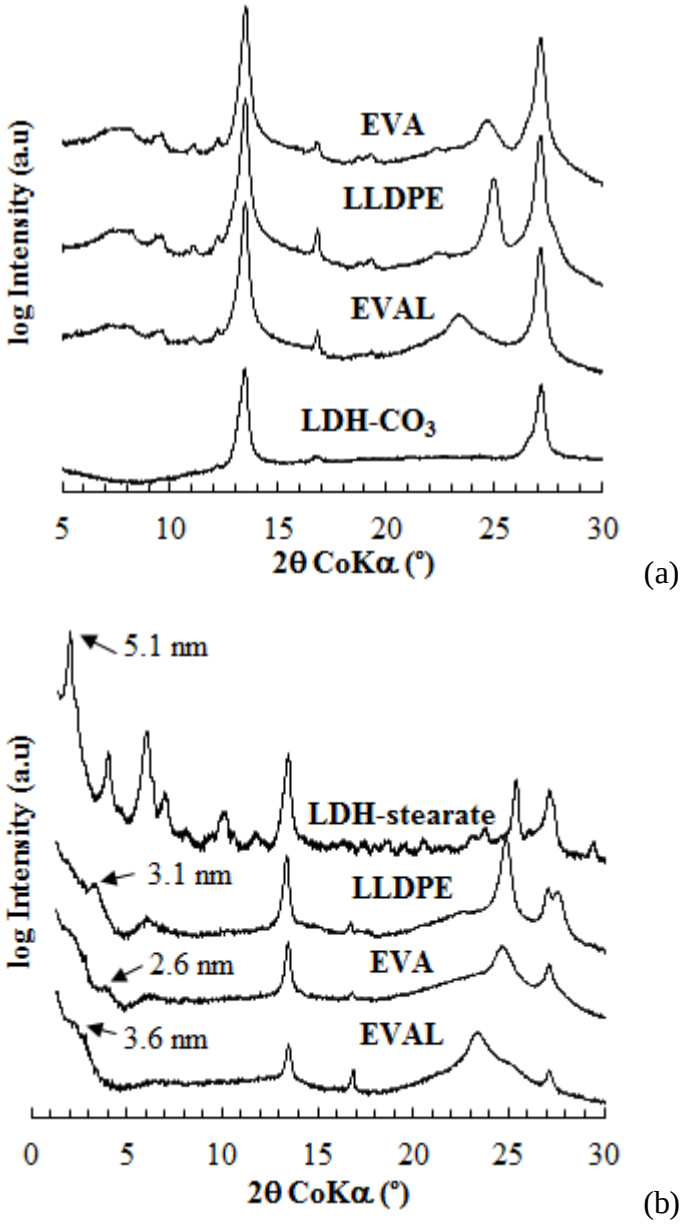

Figure 3.11. XRD diffractograms (WAXS) of the pristine, modified LDH and the 10 wt.% polymer composites indicating the relevant basal spacing

The degree of clay layer separation in the modified LDHs and the clay dispersion in the polymer composite was studied by X-ray diffraction (XRD) (Figure 3.11). The 2θ values of 13.5 and 27.2 °, which are typical for LDH-CO_3, indicate a d-spacing (d_L) of 0.76 nm. These reflections were also observed in the LDH-stearate, indicating LDH-CO_3 as an impurity phase. They were also noted in all the LDH-CO_3 and LDH-stearate polymer

composites, indicating that either this clay phase was retained during melt compounding or more of it was generated by decomposition of the LDH-stearate. The diffractogram for LDH-stearate showed three basal reflections positioned at 2.0°, 4.1° and 6.1°, the 2θ value corresponding to a d-spacing of 5.1 nm. This is consistent with bilayer intercalation of stearate moieties beyond the anion-exchange capacity of the clay (Nhlapo *et al.*, 2008). These diffractions were absent in the diffractograms of the LDH-stearate composites. The first reflection observed at high 2θ values indicated a reduction in the d-spacing of the LDH-stearate in the EVA and LLDPE composites (Figure 3.11b). The interlayer spacing of 3.1 nm determined for the LLDPE composite is consistent with monolayer-intercalated stearic acid (Xu & Braterman, 2010; Braterman *et al.*, 2004). This collapse in the d-spacing implies that the neutral stearic acid molecules, initially present in the interlayer beyond the AEC, were removed during the melt compounding process. As discussed in the Section 3.1, this was expected in view of the results obtained by Nhlapo *et al.* (2008). A collapse was also observed in the d-spacing value for the clay in the EVA composite. However, here the d-spacing was lower and this could be due to a less ordered arrangement of the intercalated chains and/or the loss of the interlayer water. Vestiges of the LDH-stearate reflections were seen in the EVAL composite. Finally, reflections typical for LDH-CO_3 were present in all composite diffractograms. This is attributed to the impurity of the LDH-stearate but it is possible that some could have formed by decomposition of the LDH-stearate during melt processing of the polymer composite. In summary, the XRD data indicated that the LDH-based polymer composites contained two types of filler particle (LDH-CO_3 and monolayer stearate-intercalated LDH) dispersed within the polymer matrices. Furthermore, no evidence for co-intercalation of polymer chains was found.

The neat polymer samples had basal reflections at 2θ values of 23.4°, 24.7° and 25.0° for EVAL, EVA and LLDPE respectively. In the composites these peaks appear to be broader and of reduced intensity. This indicates that the incorporation of LDHs increased the disorder in the packing of polymer chains during crystallisation. Eckel and Blaogh (2004) observed similar behaviour in their clay-based polymer nanocomposites, indicating that there was increased disorder in the polymer matrix.

However, as discussed in the literature review (Section 3.2), XRD analysis alone is insufficient for the assessment of the degree of dispersion in the polymer composite. TEM is used as a visual confirmation of the results obtained from XRD.

3.6.2 Transmission electron microscopy (TEM)

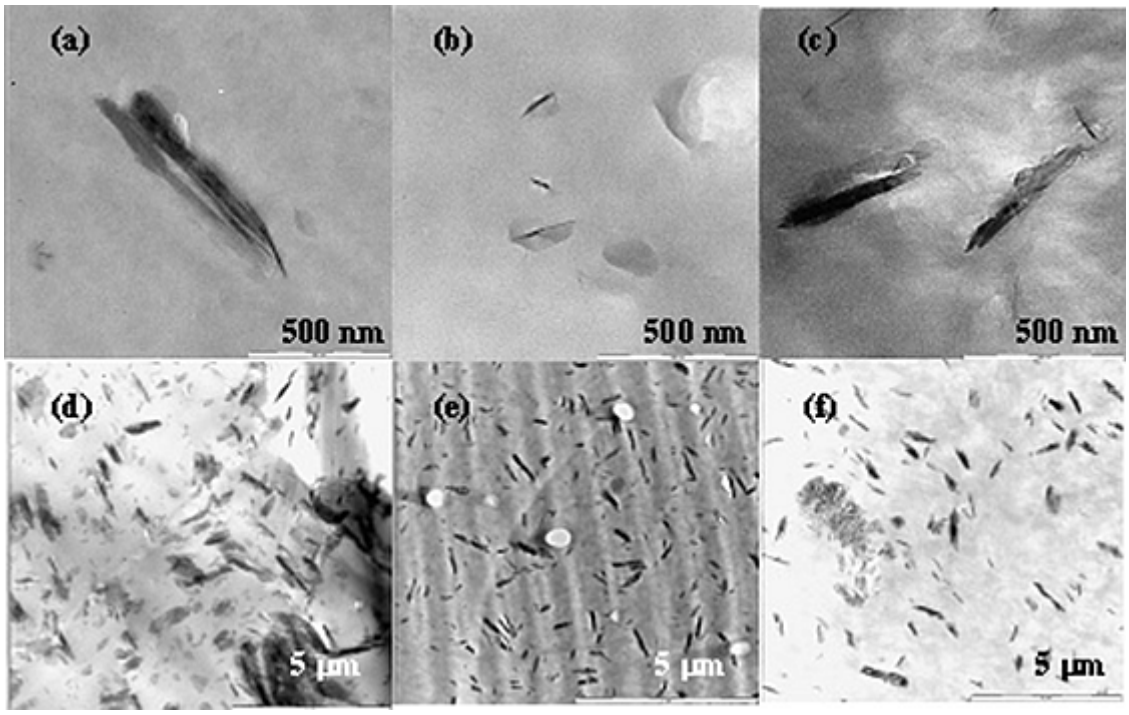

Figure 3.12. TEM images of the 10 wt.% polymer/LDH composites of (a) EVA/ LDH-St; (b) EVAL/LDH-St; (c) LLDPE/LDH-St; (d) EVA/LDH-CO_3; (e) EVAL/LDH-CO_3 and (f) LLDPE/ LDH-CO_3

The LDH-CO_3 composites featured distinct particles in the sub-micrometre range, but also some particle agglomerates (Figure 3.12 and 3.13). In the LDH-stearate composites the filler particles were much smaller, whereas in powder form they featured much larger platelets ranging up to 10 µm. They appeared as planar tactoids with a length up to about 500 nm, but with a thickness of less than 100 nm (Figure 3.12). This considerable reduction in dimensions has two possible origins. LDH platelets are weaker and less rigid than smectite clays and hence more prone to breakage. Each LDH sheet is composed of three atomic layers, whereas layered silicates have 6 to 7 atomic layers; hence LDHs tend to rupture under the shear action during extrusion (Solin *et al.*, 1995). Apart from such breakage, partial delamination may have occurred during the high-shear compounding process. The EVA and LLDPE matrices of the LDH-stearate composites appeared to contain very few tactoids. In summary, the TEM results showed that a combination of microcomposites and nanocomposites were obtained using LDH-CO_3 and LDH-stearate as fillers in the polymer matrices considered.

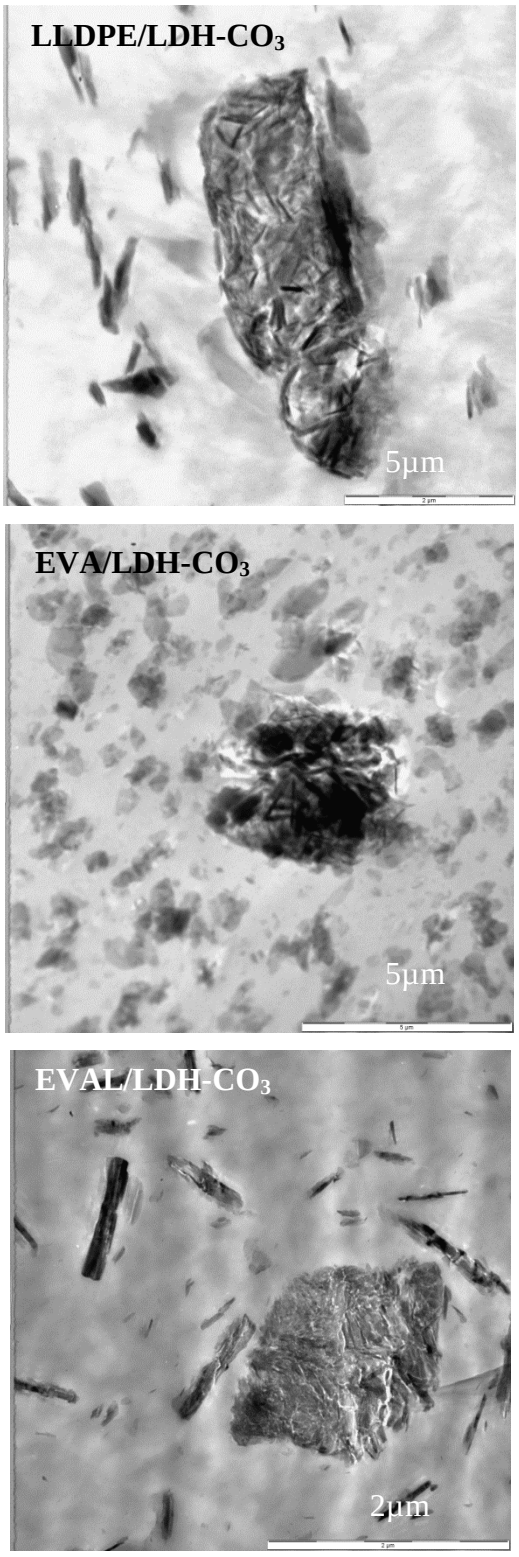

Figure 3.13. Agglomeration observed in the different matrices in SEM micrographs

The matrices of LDH-CO_3 were characterised by the existence of agglomerates/tactoids as those are shown in all the 10wt.% composites (Figure 3.13). One factor in favour of this observation is the differences in polarity between the polymer and the LDH. LDHs contain hydroxyl groups that render them polar and hence they are more compatible with polar polymer matrices, e.g. EVAL. The LDH-CO_3/EVAL composite appears to have agglomerated LDH platelets; this could be due to the high charge density which exists within the layer, hence not permitting effective dispersion/exfoliation (Adachi-Pagano *et al.*, 2000; Leroux *et al.*, 2001; Hibino & Jones, 2001). Another contributing factor is the particle-particle interactions; these are usually strong as a result of the interaction of hydroxyl groups. These interactions can either be face-to-edge ('house-of-cards' structure) or edge-to-edge. Gursky *et al.* (2006) attributed the former arrangement to lack of coordination in microscale LDH particles. A greater effect is experienced at the edges, ultimately influencing edge-to-surface interactions (see Figure 3.14).

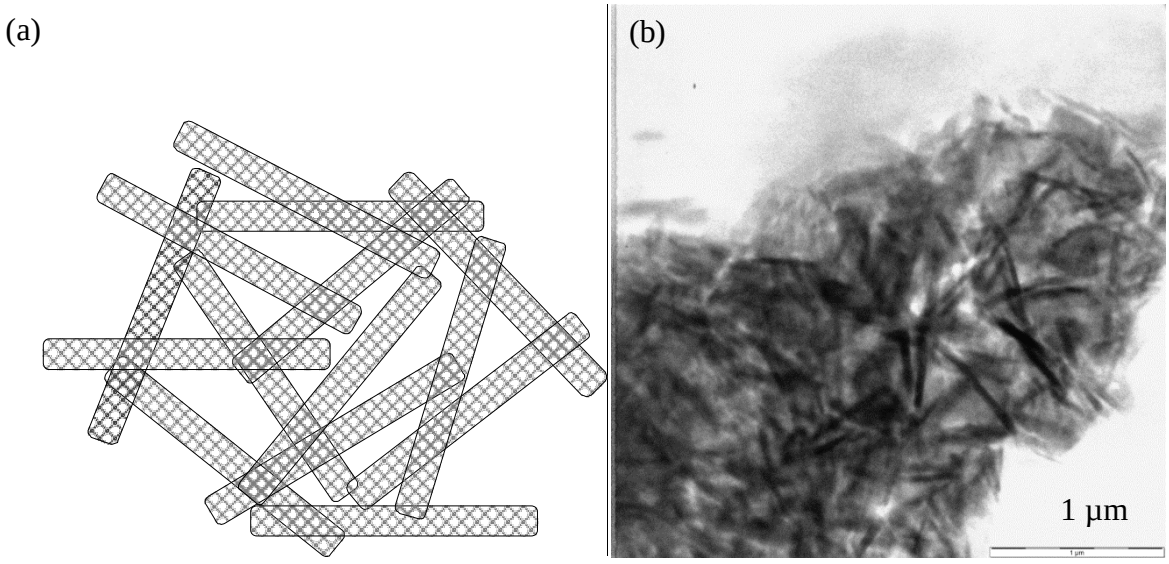

Figure 3.14. Schematic of the 'house-of-cards' structure: (a) LLDPE/LDH-CO_3 showing an agglomerate with face-to-edge interactions and (b) with edge-to-edge interactions

3.6.3 Melt viscosity

It is worth noting that the results obtained are for the polymers and composites prepared without processing aids or other additives.

Figure 3.15 presents the melt viscosity results for the composites obtained at 190 °C. All the samples showed strong shear-thinning behaviour. The EVA and EVAL polymer/LDH-CO_3 composites featured higher apparent viscosity values than the parent polymers. The melt viscosity of the LLDPE/LDH-CO_3 composite was marginally higher than that of the neat polymer. This is attributed to weak interactions between the polar filler surface and the non-polar matrix. The unmodified LDH is hydrophilic owing to the external hydroxyl groups. This results in platelet interactions such as edge-to-face or 'house of cards' arrangement, which is clearly demonstrated in Figure 3.14. This microstructure leads to high viscosities at low shear and is possibly responsible for the high viscosities observed in the LDH-CO_3 polymer composites. As the shear rates increase, the platelet aggregation breaks down and the platelets align themselves to the direction of flow, hence recording a low viscosity or one close to that of the neat polymer. The apparent melt viscosities of the EVA and the LLDPE polymer/LDH-stearate composites were lower than that of the neat polymers. This is attributed to the lubricating effect of the exuded stearic acid present in these compounds.

The EVAL/LDH-stearate composite had the highest melt viscosity. This means that the interaction of the filler with the polymer chains must have overwhelmed the lubricating effect of the free stearic acid present. The surfaces of the LDH-stearate filler are partially covered with the chains of the electrostatically attached stearate anions. So it is expected that the interaction of these clay surfaces with the EVAL chains would be weaker than the interactions with the uncoated surfaces of the LDH-CO_3 particles. However, the melt viscosity of the LDH-CO_3 composite was lower, despite its higher surface polarity. Furthermore, according to the TG results, the inorganic content of the LDH-stearate is only 20 wt.%. Taking this into consideration, these observations suggest that the clay surface area available for interaction with the polymer chains must have been much higher for LDH-stearate.

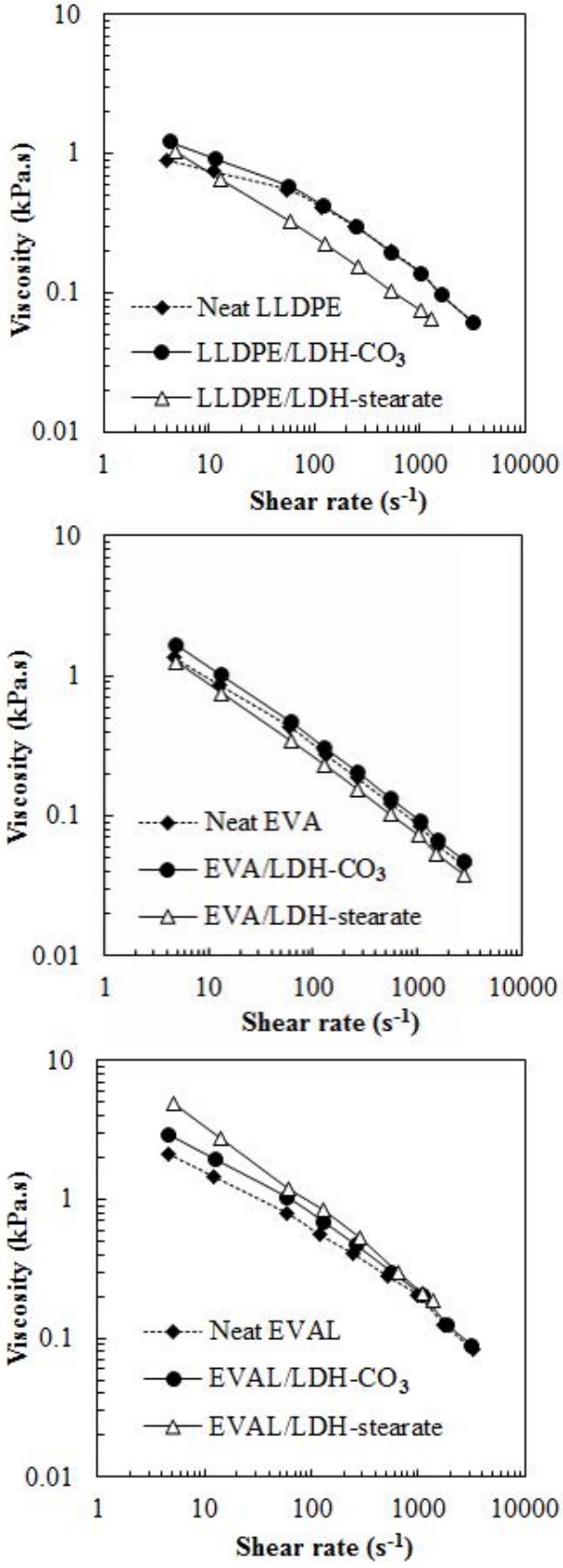

Figure 3.15. Effect of LDH incorporation on the viscosity of the polymers LLDPE, EVA and EVAL at 190 °C

3.6.4 Viscoelastic properties

Figures 3.16 to 3.18 present the DMA viscoelastic properties of the 10 wt.% composites. Results for the 5 wt.% composite may be found in Appendix C. The storage moduli (E′) of all the LLDPE (Figure 3.16), EVA (Figure 3.17) and EVAL composites (Figure 3.18) were slightly higher than that those of the neat polymer. This stiffening effect was more pronounced in the rubbery region than in the glassy region for both the EVA and EVAL composites. However, at higher temperatures the LLDPE/LDH-stearate deviated from the LDH-CO_3 composite trend and approached the behaviour of the neat polymer. This could be explained by the melting of the free stearic acid present and it acting like a plasticiser and lubricant, which facilitates the motion of the polymer chains.

The glass transition temperature (T_g) of the EVA composites was the same as that of the neat polymer. However, the T_g of the EVAL composites shifted to higher temperatures. There are two possible explanations for this observation. The exuded stearic acid might have had an anti-plasticisation effect or the mobility of the EVAL polymer chains might have been be affected by strong interactions with the surface of the filler particles. Clearly, only the latter explanation can hold for the LDH-CO_3 composite as no stearic acid was present. Based on the viscosity behaviour of the EVAL/LDH-stearate composite, it can be concluded that this explanation also holds for this system.

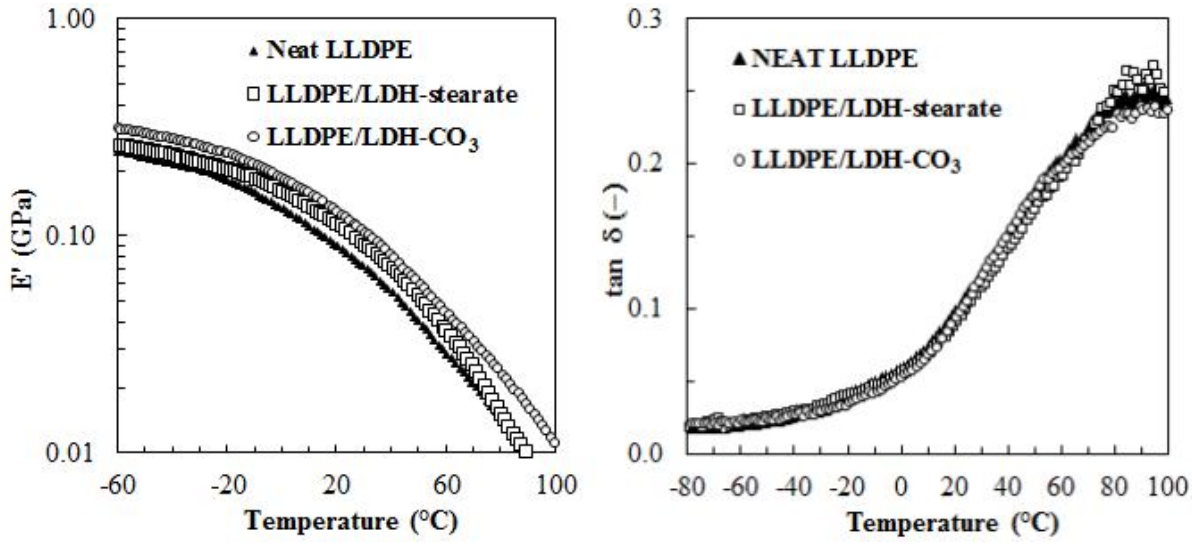

Figure 3.16. DMA data for the storage modulus and tan δ of LLDPE and its 10 wt.% derivative composites

The storage modulus for the LLDPE composites (Figure 3.16) was higher than that of the neat polymer within both the glassy and rubbery regions. However, as the temperature increased, the LLDPE/LDH-St deviated from the LDH-CO_3 composite, conforming to a behaviour similar to that of the neat polymer. This could be explained by the probable melting of excess stearic acid, which in turn acts as a plasticiser and lubricant. This facilitates the motion of polymer chains. The damping factor (tan δ) remained unchanged, signifying poor interfacial adhesion between the fillers and the polymer matrix. A similar trend is observed with the EVA composites, where the storage modulus is higher than that of the neat polymer in both regions.

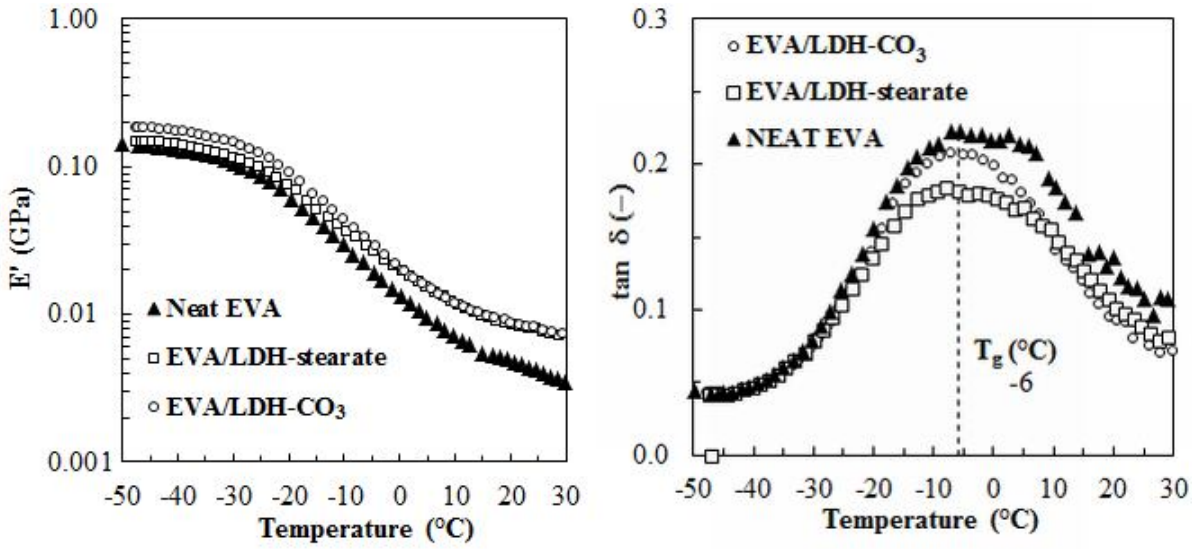

Figure 3.17. DMA data for the storage modulus and tan δ of EVA and its 10 wt.% derivative composites

The storage modulus (E′) of the EVA composite matrices (Figure 3.17) was slightly higher than that of the neat polymer in the glassy region. However, in the rubbery region the storage modulus is distinctly higher, indicating that the incorporation of the filler yields a stiffer material. The T_g of the composites was the same as for the neat polymer. This implies that the inclusion of LDHs within its matrix did not interfere with the molecular motion of the polymer chains. It also points to minimal interaction between the filler and the polymer. However, the EVA/LDH-St composite showed a reduction in the maximum tan δ value, implying that the modification of the LDH with stearate anions improves interaction between the filler and the polymer.

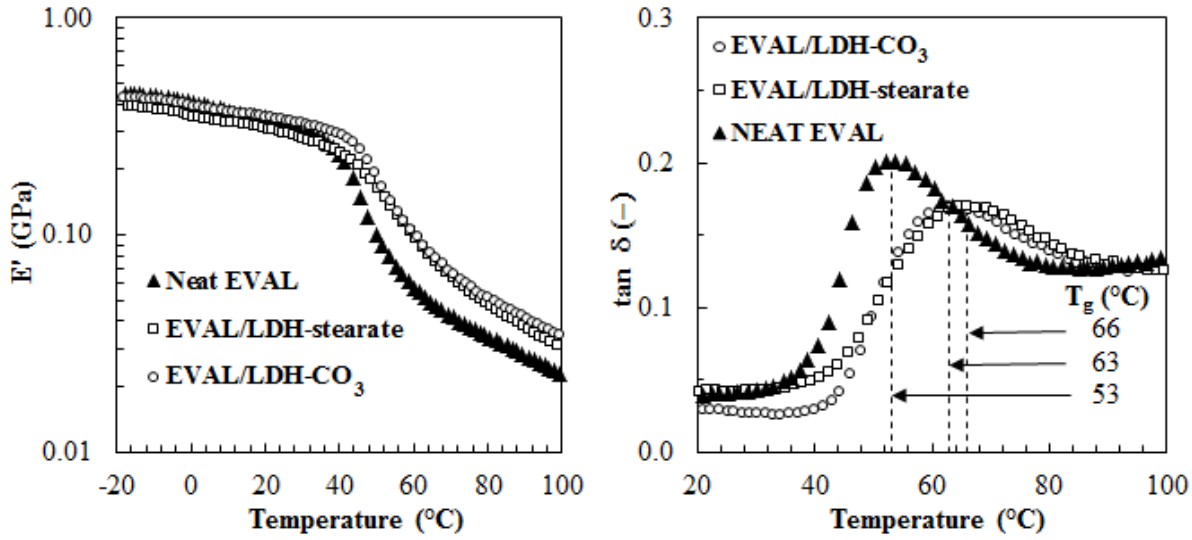

Figure 3.18. DMA data for the storage modulus and tan δ of EVAL and its 10 wt.% derivative composites

The storage modulus for the EVAL/LDH-St composite (Figure 3.18) was slightly lower than that of LDH-CO_3, which is attributed to the plasticising effect of the free stearic acid. The EVAL composites appear to have strong interfacial adhesion between the filler and the polymer, resulting from the probable formation of hydrogen bonds between the EVAL side groups and the LDH hydroxyl. This is demonstrated by restricted segmental motion, which leads to a positive shift and broadening of the tan δ peak. It is also accompanied by a decrease in the tan δ_{max} value. The T_g of the LDH-St composite is higher than that of the LDH-CO_3 due to the probable interaction of LDH hydroxyl groups and stearate anions with the polymer matrix.

3.6.5 Mechanical properties

The mechanical properties are listed in Table 3.5 and Appendix C. All the filled samples, except for the EVAL/LDH-St composite, featured higher tensile moduli than the neat polymers. Both LDHs fillers had a reinforcing effect on EVA and LLDPE as both the yield strength and the modulus increased. Enhanced elongations were obtained in the EVA composites, but a decrease was observed for the EVAL and LLDPE composites. The LLDPE/LDH-St 5 wt.% featured an outstanding increase in tenacity.

Table 3.5. Summary of the mechanical properties of LDH/polymer composites

Polymer composite	Young's modulus/ (MPa)	Yield strength (MPa)	Elongation at break (%)	Charpy impact strength/ (kJ/m^2)	Tensile impact strength/ (kJ/m^2)
EVA					
Neat EVA	27 ± 2	10 ± 0.4	277 ± 30	No break	3.8 ± 0.1
EVA / 5% LDH-St	34 ± 3	11 ± 0.1	330 ± 12	-	4.6 ± 0.3
EVA / 10%LDH-St	40 ± 5	12 ± 0.1	422 ± 23	No break	4.3 ± 0.2
EVA / 5% LDH-CO_3	30 ± 1	10 ± 0.1	305 ± 12	-	3.4 ± 0.1
EVA/10% LDH-CO_3	37 ± 2	13 ± 1	424 ± 60	No break	5.2 ± 0.1
LLDPE					
Neat LLDPE	171 ± 14	16 ± 0.1	509 ± 29	22 ± 2	1.7 ± 0.1
LLDPE / 5%LDH-St	192 ± 6	24 ± 3	1097 ± 14	-	1.1 ± 0.1
LLDPE / 10%LDH-St	196 ± 7	17 ± 0.4	495 ± 43	12 ± 1	1.2 ± 0.1
LLDPE / 5%LDH-CO_3	219 ± 43	17 ± 0.2	477 ± 13	-	1
LLDPE/10%LDH-CO_3	213 ± 12	17 ± 0.2	460 ± 21	11 ± 1	0.8 ± 0.1
EVAL					
Neat EVAL	843 ± 16	64 ± 2	41 ± 21	4.9 ± 1	2 ± 0.3
EVAL / 5%LDH-St	869 ± 23	71± 0.2	42 ± 4	-	1.8 ± 0.3
EVAL / 10%LDH-St	718 ± 40	59 ± 6	18 ± 5	9.7 ± 3	0.8 ± 0.3
EVAL / 5% LDH-CO_3	969 ± 22	77 ± 1	31 ± 1	-	0.8 ± 0.3
EVAL / 10%LDH-CO_3	1025 ± 18	76 ± 0.4	37 ± 2	4.6 ± 1	0.7 ± 0.3

Polymer toughness is governed by parameters such as the degree of particle dispersion within the polymer matrix, filler mobility, delamination and intrinsic changes to polymer properties promoted by the filler (Chen *et al.*, 2008). The EVA composites did not fracture in the notched Charpy tests because of the rubbery nature of the matrix. The tests were basically carried out at room temperature, so well above the T_g of this polymer matrix; in this case the mobility of the polymer chains is higher. This aspect facilitates the mobility of the LDHs to form temporary bonds which in turn dissipate energy. Hence the clay platelets are able to rotate and align themselves in the direction of the applied stress. During the matrix deformation process, the filler is squeezed tight by the cavity walls as it elongates and narrows. The resulting friction forces generate a region of enhanced strength which

retards the growth of the cavity and thus delays polymer failure (Gersappe, 2002). The tensile impact properties of the filled EVA composites were better than those of the neat polymer. However, the opposite was true for the other polymer matrices. In the tensile strength impact tests the LDH-CO_3 filler gave better results than the LDH-St (see Table 3.5). Considering Figure 3.8, this can be attributed to better interfacial adhesion between the polar filler and the polar EVA matrix.

With the exception of the 10 wt.% EVAL/LDH-St composite, all the other composite samples had poor notched Charpy impact properties compared with the parent polymers. Development of strong energy dissipation mechanisms is a prerequisite for good impact properties. The poor interface adhesion between both the fillers and the polyethylene matrix is evident in Figure 3.10. This means that the incorporation of the fillers led to the creation of internal flaws. These acted as stress concentrators which led to premature mechanical failure. The LLDPE/LDH-St composite had slightly better impact strength properties than the LLDPE/LDH-CO_3. This can be attributed to the slightly better compatibility with the polymer matrix contributed by the exuded stearic acid coating on the LDH particles (Figure 3.10). However, it is clear from the XRD diffractogram (Figure 3.11) that the presence of this filler also affected the morphology of the parent polymer. This is confirmed by the broadening and shift in position of the main reflections attributable to the polymer matrix. This change in the morphology of the polymer matrix could also have affected the impact properties.

Unexpectedly, the notched Charpy impact strength of EVAL increased from 4.9 kJ m^{-2} to 9.7 kJ m^{-2} when 10 wt.% LDH-stearate was added (Table 3.5). Top-view SEM imaging of the fracture surfaces was inconclusive. The images did not reveal a mechanism that could explain the improved impact behaviour. Figure 3.19 shows side-view images of the fracture surfaces of Charpy impact specimens obtained for the EVAL composites using an optical microscope. The neat EVAL sample and EVAL/LDH-CO_3 composite sample showed clean fractures. In contrast, the EVAL/LDH-St sample showed an extensive stress-whitened damage region which extended deep into the sample. It seems that the clay particles transmitted an incoming crack as multiple crack fronts travelling in different directions. This dissipates mechanical energy by creating numerous internal cracks with a very large total surface area. This ability of the LDH-stearate might derive from its sheet-like nature and random orientation in the glassy matrix. It is noteworthy that the stress-whitened

damage region was located in a narrow region towards the back of the sample. Extensive stress whitening is usually an indication of crazing and/or microfibril formation. The white appearance of the crazed region is due to light scattering.

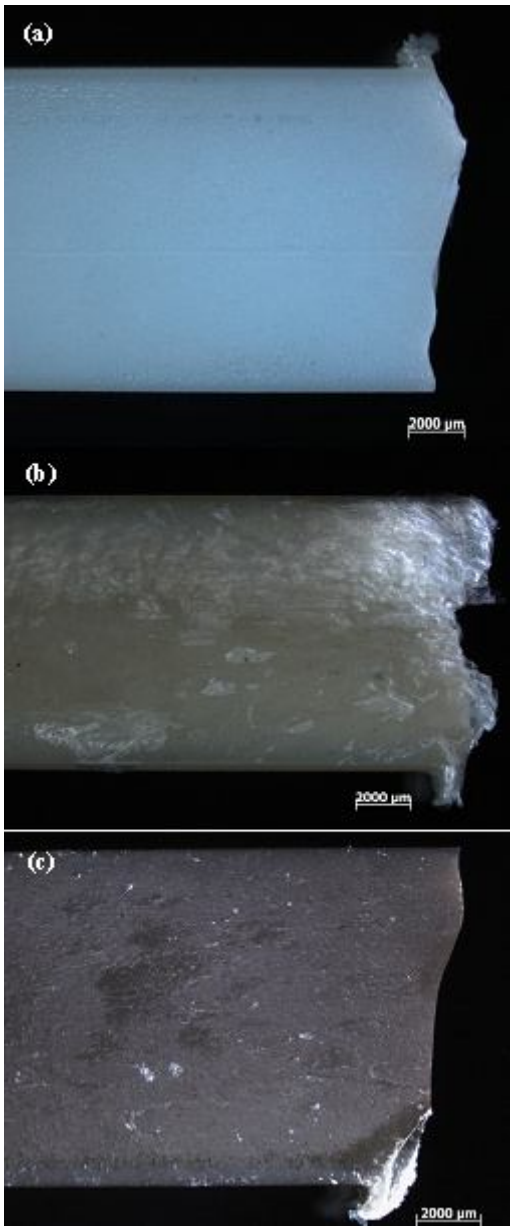

Figure 3.19. Optical light microscope side-views of Charpy impact test specimen of EVAL: (a) neat, (b) LDH-stearate composite and (c) LDH-CO_3 10 wt.% composite

However, for the tensile impact specimen there is a clear indication of debonding and the matrix has areas of extensive fibrillation (see Figure 3.20). More views are shown in Appendix C.

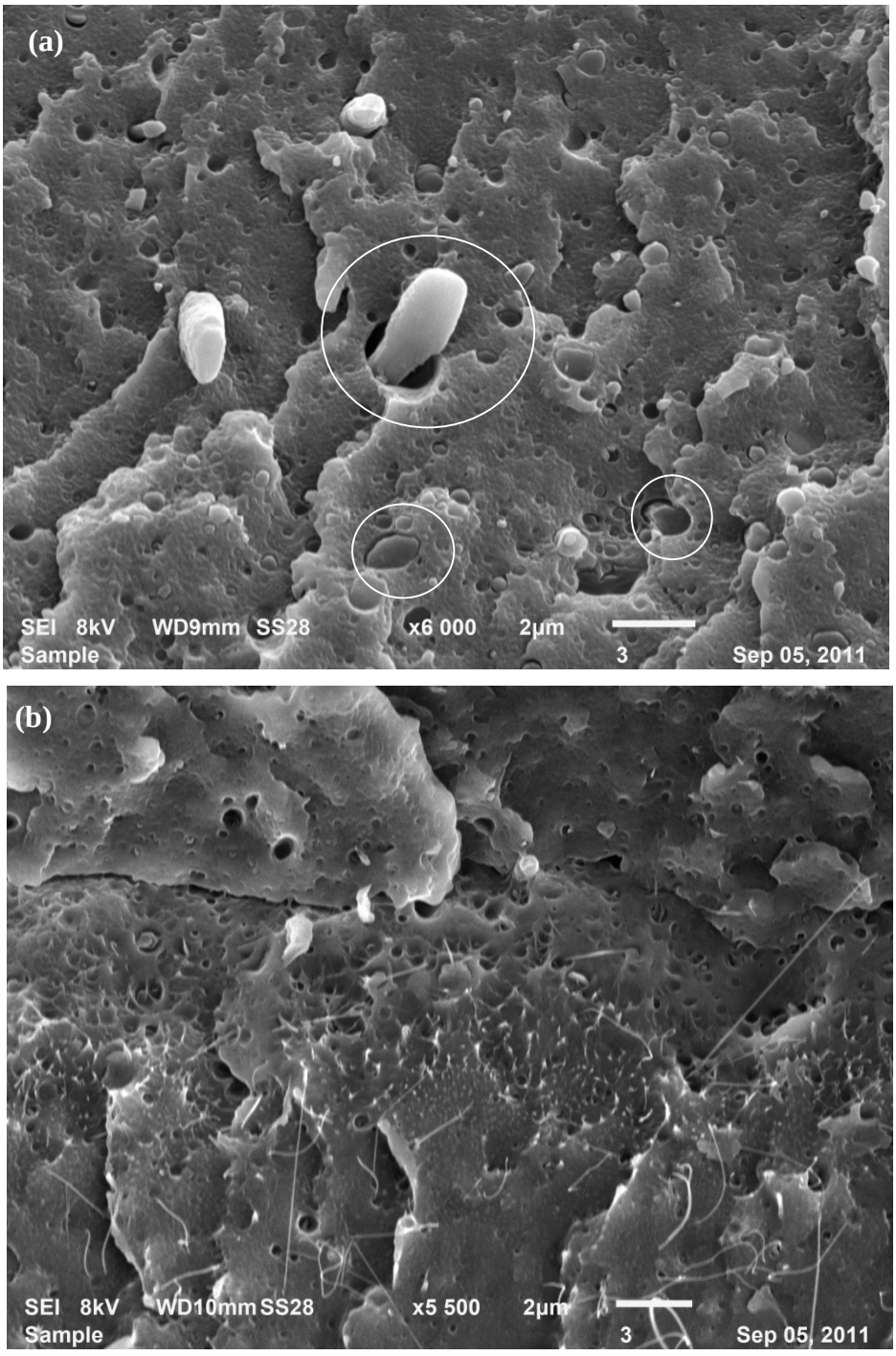

Figure 3.20. Top view of the EVAL/LDH-St tensile impact test specimen showing: (a) debonding and (b) fibrillation

3.6.6 Thermal analysis

The thermal data are summarised in Table 3.6, comparing the temperature changes at 10 and 50% weight loss between the neat polymers and composite samples, i.e. $T_{0.1}$ and $T_{0.5}$ respectively. The addition of LDHs within the different polymer matrices improves the thermal stability at $T_{0.1}$ and $T_{0.5}$, with an increase in the char residue levels in all composite samples. The thermal degradation temperature for the EVA and LLDPE composites was 2-16 °C above that of the neat polymers. However, the improvement was less for the EVA when compared with the LLDPE matrix. EVA and its composites undergo two main thermal events, the first occurring between 220 and 405 °C due to deacetylation with the release of gaseous acetic acid, and the final event as a result of main chain scission (between 410 and 510 °C) associated with polyolefinic groups (Camino *et al.*, 2000; Riva, 2002; Peeterbroeck *et al.*, 2005; Jiao *et al.*, 2006).

Table 3.6. Thermal stability data at $T_{0.1}$, $T_{0.5}$, % residue and change in temperature (ΔT), results pertaining to 10 wt.% composites

Sample	$T_{0.1}$ (°C)	$T_{0.5}$ (°C)	Residue (%)	$\Delta T_{0.1}$(°C)	$\Delta T_{0.5}$(°C)
Neat EVA	350	438	0		
EVA/LDH-St	349	447	1.4	-1	9
EVA/LDH-CO_3	353	440	6.0	3	2
Neat EVAL	370	406	0		
EVAL/LDH-St	291	309	1.5	-79	-97
EVAL/LDH-CO_3	296	315	5.4	-74	-91
Neat LLDPE	387	426	0		
LLDPE/LDH-St	381	441	2.0	-6	15
LLDPE/LDH-CO_3	403	442	5.8	16	16

In the EVAL samples the first event occurs at about 358 °C and the same applies for all the composite samples (see Figure C-16 in Appendix C). The second event is shifted to a higher temperature, from 440 °C to 443 and 453 °C for the EVA/LDH-St and LDH-CO_3 composites respectively. The EVA/LDH-CO_3 composite showed greater thermal stability at $T_{0.5}$ than the neat polymer. A marked difference is observed in the EVAL composites where

the temperature difference between the onset decomposition temperatures, $T_{0.1}$ and $T_{0.5}$, is a magnitude of 88–115 °C lower than that of the neat polymer. This could be explained by the formation of metal oxides and/or radical species that catalyse the thermal degradation of the polymer; hence a significant difference is observed. In addition, it may be explained as a result of thermo-oxidative degradation of the polymer. In the thermogram (Figure 3.21), one can clearly observe the shift at which thermal degradation occurs for the EVAL composites.

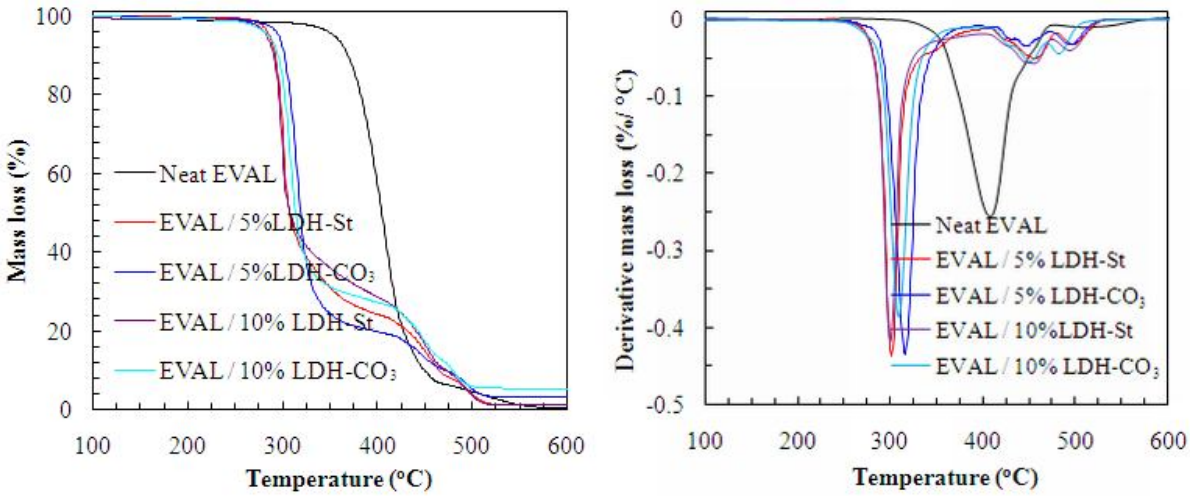

Figure 3.21. TG data for EVAL and derivative composites

3.6.6.1 Differential scanning calorimetry

Differential scanning calorimetry (DSC) was employed to study thermal transitions and follow the changes in enthalpies in the composites (see Table 3.7). The data discussed pertain to those obtained from the second heating and first cooling. There is a general increase in the melting temperature in the filled polymers. The same trend is observed in the crystallisation temperature in Figure 3.22, with the exception of the EVAL composite for which a distinct difference is observed. An increase in the crystallisation temperature of the composites of EVA and LLDPE is an indication of the nucleating effect of the LDH incorporation. However, the enthalpy of the melting endotherms of the polymer composites decreases; this is a result of a decrease in crystallinity or a change in the ordering of the polymer chains induced by the filler materials (Ramaraj & Yoon, 2008). It is established that fillers can affect the crystallinity of some polymers, and consequently affect their mechanical properties. An inverse correlation was obtained between the nucleating ability of fillers and loss of impact strength in the filled systems (Hutley & Darlington, 1985). The

same correlation is observed in the LLDPE composites where the crystallisation temperature increases. However, the impact strength reduces by a magnitude of almost 50%, as seen in Tables 3.5 and 3.7.

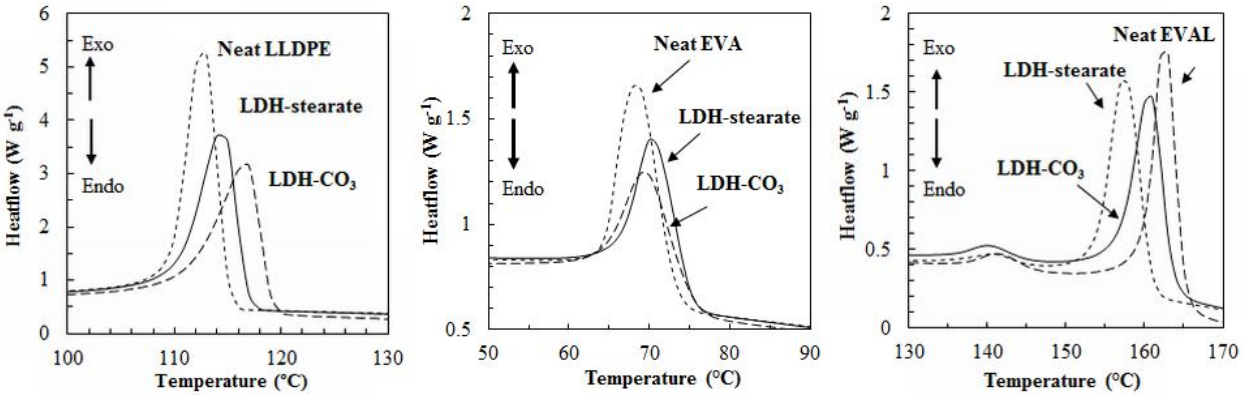

Figure 3.22. DSC cooling traces of each of the 10 wt.% polymer composite systems

To further study the nucleating effect of LDH in the LLDPE matrix, POM analyses were carried out (see Figure 3.23). The samples show a reduction in the grain size of crystallites in the composites. This is attributed to the availability of numerous nuclei (LDH particles) in the composite, resulting in very small crystallites. Though the LLDPE/LDH-CO_3 sample generally exhibits a reduced crystallite size, there are areas with large crystals which are indicated by arrows in Figure 3.23. Such big crystallites may act as stress concentrators, leading to premature fracture.

Figure 3.23. POM images of neat LLDPE and derivative composites (scale bar is 40 µm)

The same fillers retarded the crystallisation of the EVAL (Figure 3.22). This is attributed to a strong interaction of the EVAL polymer chains with well-dispersed clay platelets and the higher melt viscosity which suppresses the diffusion processes required for the chains to orient and pack into crystallites.

Table 3.7. DSC data indicating the onset temperature and melting endotherm of the 10 wt.% polymer composites

	Onset melting temperature (˚C)	**Melting temperature, T_m (°C)**	**Melting endotherm (J/g)**	**Onset of crystallisation (°C)**	**Crystallisation temperature T_c (°C)**	**Crystallisation exotherm (J/g)**
Neat EVA	60	85	55	75	70	55
EVA/LDH-St	60	85	42	76	71	46
EVA/LDH-CO_3	64	85	60	74	70	63
Neat EVAL	176	182	55	164	162	47
EVAL /LDH-St	175	183	48	161	157	46
EVAL /LDH-CO_3	175	181	45	163	161	46
Neat LLDPE	121	126	76	117	115	61
LLDPE/LDH-St	121	127	68	118	116	63
LLDPE /LDH-CO_3	120	128	67	119	117	61

3.7 CONCLUSION

Anionic clay/polymer composites were prepared by melt compounding two different LDH fillers into polyethylene random copolymers. In order of increasing polarity, the latter were 1-hexene-based LLDPE, EVA and EVAL. A standard carbonate form (LDH-CO_3) and a stearate-modified LDH (LDH-St) were used as fillers. The latter comprised a bilayer-intercalated form containing ca. 50% more stearic acid than expected from the anionic exchange capacity of the parent clay. The composite materials were characterised by XRD, SEM, TEM, TGA, DSC, DMA and capillary rheology. Mechanical testing in tensile mode and Charpy impact tests were also conducted.

During melt compounding of the LDH-stearate composites, the excess stearic acid in the clay was released and the clay reverted to a monolayer-intercalated form. This conclusion is supported by XRD data and the reduction in melt viscosity observed for the LLDPE and EVA polymer/LDH-stearate composites. The latter is caused by the lubrication effect of the free stearic acid present. The EVAL/LDH-stearate nanocomposite featured the highest melt viscosity. This suggests that the clay surface area available for interaction with the EVAL polymer chains must have been very high in the EVAL/LDH-stearate composite in order to overwhelm the lubrication effect. Such strong interaction in this system is supported by the increase in the glass transition temperature (T_g) observed by DMA.

XRD confirmed that the presence of LDH-stearate-based polymer composites contained two types of filler particle (LDH-CO_3 and monolayer stearate-intercalated LDH) dispersed within the polymer matrices. The TEM results showed that microcomposites and nanocomposites were obtained using LDH-CO_3 and LDH-St as fillers in the polymer matrices considered. SEM images of freeze-fractured surfaces indicated good interfacial adhesion between the clay and the matrix, not only in the EVAL composites, but also in the EVA/LDH-CO_3 composite.

DSC showed that the presence of the fillers interfered with the polymer crystallisation processes. Both fillers acted as nucleating agents in LLDPE and EVA. The degree of crystallinity of the EVA even improved, as shown by an increase in the enthalpy of crystallisation. The XRD results confirmed that the crystal morphology of the LLDPE was changed. Both fillers retarded the crystallisation of the EVAL. This is attributed to the strong

interaction of the EVAL polymer chains with the well-dispersed clay platelets and the higher melt viscosity, which suppresses the diffusion processes required for the chains to orient and pack into crystallites.

Both LDHs fillers had a reinforcing effect on EVA and LLDPE as both the yield strength and the modulus improved. Better elongations were obtained in the EVA composites, but a decrease was observed for the EVAL and LLDPE composites. Both fillers improved the tensile impact strength of EVA. Unexpectedly, the notched Charpy impact strength of EVAL increased significantly (from 4.9 to 9.7 kJ m^{-2}) when 10 wt.% LDH-stearate was added. This is attributed to the ability of the highly dispersed and randomly oriented nanosized clay platelets to promote extensive internal microcavitation during impact loading. The creation of a large internal surface area provided the requisite energy-dissipation mechanism.

3.8 REFERENCES

Abbasian, M. (2011). Exfloliated poly(styrene-co-methylstyrene) grafted polyaniline/layered double hydroxide nanocomposite synthesized by solvent blending method. *J. Appl. Polym. Sci.*, 122: 2573–2582.

Acharya H, Srivastava, S. K, Bhowmick A. K. (2007). A solution blending route to ethylene propylene diene terpolymer / layered double hydroxide nanocomposites. *Nanoscale Res. Lett.*, 2:1-5.

Adachi-Pagano, M., Forano, C. & Besse, J-P. (2000). Delamination of layered double hydroxides by use of surfactants. *Chem. Commun*., 13: 91–92.

Alexandre, M. & Dubois, P. (2000). Polymer-layered silicate nanocomposites: preparation, properties and uses of a new class of materials. *Mater. Sci. Eng., R.*, 28(1–2):1–63.

Bocchini, S., Morlattherias, S., Gardette, J. & Camino, G. (2008). Influence of nanodispersed hydrotalcite on polypropylene photooxidation. *Eur. Polym. J.*, 44(11): 3473–3481.

Braterman, P. S., Xu, Z. P. & Yarberry, F. (2004). In: Auerbach, S. M., Carrado, K. A. & Dutta, P. K. (Eds), *Handbook of Layered Materials*, Boca Raton: CSC Press, Taylor & Francis Group, pp 373–449.

Camino, G., Maffezzoli, A., Bragalia, M., De Lazzaro, M. & Zammarano, M. (2001). Effect of hydroxides and hydroxycarbonate structure on fire retardant effectiveness and mechanical properties in ethylene-vinyl acetate copolymer. *Polym. Degrad. Stab.*, 74(3): 457–464.

Carrado, K.A. & Xu, L. (1999). Materials with controlled mesoporosity derived from synthetic polyvinylpyrrolidone-clay composites. *Microporous & Mesoporous Mater.*, 27: 87–94

Challier, T. & Slade, R. C. T. (1994). Nanocomposite materials: Polyaniline-intercalated layered double hydroxides. *J. Mater. Chem.*, 4(3): 367–371.

Chen, B. (2004). Polymer–clay nanocomposites: An overview with emphasis on interaction mechanisms. *Br. Ceram. Trans.*, 103(6): 241–249.

Chen, B., Evans, J. R. G., Greenwell, H. C., Boulet, P., Coveney, P. V., Bowden, A. A & Whiting, A. (2008). A critical appraisal of polymer-clay nanocomposites. *Chem. Soc. Rev.*, 37(3): 568–94.

Chen, G. (2007). Preparation of a poly(vinyl chloride)/layered double hydroxide nanocomposite with a reduced heavy-metal thermal stabilizer. *J. Appl. Polym. Sci.*, 106: 817–820.

Chen, W. & Qu, B. (2003). Structural characteristics and thermal properties of synthesized by solution intercalation. *Chem. Mater.*, 15(14): 3208–3213.

Chen, W. & Qu, B. (2004). LLDPE/ZnAl LDH-exfoliated nanocomposites: Effects of nanolayers on thermal and mechanical properties. *J. Mater. Chem.*, 1705–1710.

Chiang, M.-F., Chu, M.-Z. & Wu, T.-M. (2011). Effect of layered double hydroxides on the thermal degradation behavior of biodegradable poly(l-lactide) nanocomposites. *Polym. Degrad. Stab.*, 96(1): 60–66.

Cho, J. W. & Paul, D. R. (2001). Nylon 6 nanocomposites by melt compounding. *Polymer*, 42: 1083–1094.

Coiai, S., Passaglia, E., Hermann, A., Augier, S., Pratelli, D. & Streller, R. C. (2010). The influence of the compatibilizer on the morphology and thermal properties of polypropylene-layered double hydroxide composites. *Polym. Compos.*, 1–11.

Costa F. R., Saphiannikova M., Wageknecht, U. & Heinrich, G. (2008) Layered double hydroxide based polymer nanocomposites. *Adv. Polym. Sci.*, 210: 101–168.

Costa, F. R., Abdel-Goad, M., Wagenknecht, U. & Heinrich, G. (2005). Nanocomposites based on polyethylene and Mg-Al layered double hydroxide. Part I: Synthesis and characterization. *Polymer*, 46: 4447–4453.

Costa, F. R., Wagenknecht, U. & Heinrich, G. (2007). LDPE/Mg–Al layered double hydroxide nanocomposite: Thermal and flammability properties. *Polym. Degrad. Stab.*, 92(10), 1813–1823.

Costa, F. R., Wagenknecht, U., Jehnichen, D., Abdel-Goad, M. and Heinrich, G. (2006). Nanocomposites based on polyethylene and Mg-Al layered double hydroxide. Part II: rheological characterization. *Polymer*, 47: 1649–1660.

Costache, M. & Wang, D. (2006). The thermal degradation of poly(methyl methacrylate) nanocomposites with montmorillonite, layered double hydroxides and carbon nanotubes. *Polym. Adv. Technol.*, 17: 272–280.

Cui, W., Jiao, Q., Zhao, Y., Li, H., Liu, H. & Zhou, M. (2012).Preparation of poly (ethylene terephthalate)/ layered double hydroxide nanocomposites by in-situ polymerization and their thermal property. *Express Polym. Lett.*,6(6): 485-493

Du, L. & Qu, B. (2006). Structural characterization and thermal oxidation properties of LLDPE/MgAl-LDH nanocomposites. *J. Mater. Chem.*, 3: 1549–1554.

Du, L., Qu, B. & Zhang, M. (2007). Thermal properties and combustion characterization of nylon 6/MgAl-LDH nanocomposites via organic modification and melt intercalation. *Polym. Degrad. Stab.*, 92(3): 497-502.

Eckel, D. & Balogh, M. (2004). Assessing organo-clay dispersion in polymer nanocomposites. *J. Appl. Polym. Sci.*, 93: 1110–1117.

Fischer, H. (2003). Polymer nanocomposites: From fundamental research to specific applications. *Mat. Sci. Eng. C.*, 23: 763–772.

Focke, W. W., Nhlapo, N. S., Moyo, L. & Verryn, S. M. C. (2010). Thermal properties of lauric- and stearic acid intercalated layered double hydroxides. *Mol. Cryst. Liq.Cryst.*, 521(1): 168–178.

Gao, F., Chen, S., Hull, J.B. (2001). Layer expansion of layered silicates in solid polymer matrices by compression. *J. Mater. Sci. Lett.* 20, 1807–1810.

Gersappe, D. (2002). Molecular mechanisms of failure in polymer nanocomposites. *Phys. Rev. Lett.*, 89(5): 58301–5830.

Gursky, J. A, Blough, S. D., Luna, C., Gomez, C., Luevano, A. N. & Gardner, E. A. (2006). Particle-particle interactions between layered double hydroxide nanoparticles. *J. Amer. Chem. Soc.*, 128(26): 8376–8377.

Hancock, M. (1995). Particulate filled polymer composites, Chapter 8. In: Rothon, R. N. (Ed.), *Particulate Filled Polymer Composites'*, Harlow, UK: Longman Scientific and Technical.

Herrero, M., Martínez-Gallegos, S., Labajos, F. M. & Rives, V. (2011). Layered double hydroxide/polyethylene terephthalate nanocomposites. Influence of the intercalated LDH anion and the type of polymerization heating method. *J. Solid State Chem.*, 184(11): 2862–2869.

Hibino, T. & Jones, W. (2001). New approach to the delamination of layered double hydroxides. *J. Mater Chem.*, 11(5): 1321–1323.

Hsueh, H.-B. & Chen, C.-Y. (2003). Preparation and properties of LDHs/epoxy nanocomposites. *Polymer*, 44: 5275–5283.

Huang, S., Cen, X., Zhu, H., Yang, Z., Yang, Y., Tjiu, W. W. & Liu, T. (2011). Facile preparation of poly(vinyl alcohol) nanocomposites with pristine layered double hydroxides. *Mater. Chem. Phys.*, 130(3): 890–896.

Hutley, T. J. & Darlington, M. W. (1985). Further observation on impact strength-DSC correlation in mineral filled polypropylene. *Polym. Commun.*, 26: 264–267

Isupov, V. P., Chupakhina, L. E., Ozerova, M. A., Kostrovsky, V. G. & Poluboyarov, V. A. (2001). Polymerization of m-$NH_2C_6H_4COO$ anions in the intercalation compounds of aluminium hydroxide $[LiAl_2(OH)_6]$[m-$NH_2C_6H_4COO]\cdot nH_2O$. *Solid State Ionics*, 141–142: 231–236.

Jiao, C. M., Wang, Z. Z., Ye, Z., Hu, Y. & Fan, W. C. (2006). Flame retardation of ethylene-vinyl acetate copolymer using nano magnesium hydroxide and nano hydrotalcite. *J. Fire Sci.*, 24: 47–64.

Katiyar, V., Gerds, N., Koch, C. B., Risbo, J., Hansen, H. C. B. & Plackett, D. (2011). Melt processing of poly(L-lactic acid) in the presence of organomodified anionic or cationic clays. *J. Appl. Polym. Sci.*, 122: 112–125.

Kawasumi, M. (2004). The discovery of polymer-clay hybrids. *J. Polym. Sci. Part A: Polym. Chem.*, 42(4): 819–824.

Khan, A. & O'Hare, D. (2002). Intercalation chemistry of layered double hydroxides: Recent developments and applications. *J. Mater. Chem.*, 12: 3191–3198.

Kim, G.M. & Michler, G.H. (1998). Micromechanical deformation process in toughened and particle-filled semicrystalline polymers: Part 1. Characterization of deformation processes in dependence on phase morphology. *Polymer*. 39: 5689–5697.

Kotal, M., Kuila, T., Srivastava, S. K. & Bhowmick, A. K. (2009). Synthesis and characterization of polyurethane/Mg-Al layered double hydroxide nanocomposites. *J. Appl. Polym. Sci.*, 114: 2691–2699.

Kuila, T. & Acharya, H. (2007). Synthesis and characterization of ethylene vinyl acetate/Mg–Al layered double hydroxide nanocomposites. *J. Appl. Polym. Sci.*, 1–7.

Kuila, T., Srivastava, S. K., Bhowmick, A. K. & Saxena, A.K. (2008) . Thermoplastic polyolefin based polymer-blend-layered double hydroxide nanacomposite. J.Comp. Sci. Tech., 68: 3234-3239

Lee, W.D., Im, S.S., Hyung-Mi, L. & Kwang-Jin, K. (2006). Preparation and properties of layered double hydroxides/poly(ethylene terephthalate) nanocomposites by direct melt compounding. *Polymer*. 47: 1364-1371

Lee, J. H., Nam, J., Rhee, W. & Jung, D. (2008). Hybrid assembly of layered double hydroxide nanocrystals with inorganic , polymeric and biomaterials from micro- to nanometer scales. *Euro. J. Inorg. Chem*, 5573–5578.

Lee, W.D. & Im, S.S. (2007). Thermomechanical properties and crystallization behaviour of layered double hydroxides/poly(ethylene terephthalate) nanocomposites prepared by in-situ polymerization. *J. Polym. Sci., Part B: Polym. Phys.* 45, 28–40.

Leroux, F., Adachi-Pagano, M., Intissar, M., Chauvière, S., Forano, C. and Besse, J-P. (2001). Delamination and restacking of layered double hydroxides. *J. Mater. Chem.*, 11: 105–112.

Liu, J., Chen, G. & Yang, J. (2008). Preparation and characterization of poly(vinyl chloride)/layered double hydroxide nanocomposites with enhanced thermal stability. *Polymer*, 49(18): 3923–3927.

Liu, J., Chen, G., Yang, J. & Ding, L. (2009). Improved thermal stability of poly(vinyl chloride) by nanoscale layered double hydroxide particles grafted with toluene-2, 4-di-isocyanate. *Mater. Chem. Phys.*, 118: 405–409.

Lonkar, S. P., Morlat-Therias, S., Caperaa, N., Leroux, F., Gardette, J. L. & Singh, R. P. (2009). Preparation and nonisothermal crystallization behavior of polypropylene/layered double hydroxide nanocomposites. *Polymer*, 50(6): 1505–1515.

Lonkar, S. P., Therias, S., Leroux, F., Gardette, J-L. & Singh, R. P. (2012). Thermal, mechanical and rheological characterization of polypropylene/layered double hydroxide nanocomposite. *Polym. Eng. Sci,*. 52(9): 2006–2014.

Magagula, B., Nhlapo, N. & Focke, W. W. (2009). Mn_2Al-LDH- and Co_2Al-LDH-stearate as photodegradants for LDPE film. *Polym. Degrad. Stab.*, 94(6): 947–954.

Manias, E., Polizos, G., Nakajima, H. & Heidecker, M. J. (2007) Fundamentals of polymer nanocomposites. In: Morgan, A. B. & Wilkie, C. A. (Eds), *Flame Retardant Polymer Nanocomposites*. New York: Wiley, pp 31–66.

Marangoni, R., Costa Gardolinski, J. E. F., Mikowski, A. & Wypych, F. (2010). PVA nanocomposites reinforced with Zn2Al LDHs, intercalated with orange dyes. *J. Solid State Electrochem.*, 15(2): 303–311.

MIT Open Course Ware (2009). *Polymer Physics*. Boston: MIT School of Engineering.

Moujahid, E. M., Besse, J.-P. & Leroux, F. (2002). Synthesis and characterization of a polystyrene sulfonate layered double hydroxide nanocomposite. In-situ polymerization vs. polymer incorporation. *J. Mater. Chem.*, 12(11): 3324–3330.

Moujahid, E. M., Leroux, F., Dubois, M. & Besse, J. (2003). In situ polymerisation of monomers in layered double hydroxides. *C.R. Chimie*, 6: 259–264.

Muksing, N., Magaraphan, R., Coiai, S. & Passaglia, E. (2011). Effect of surfactant alkyl chain length on the dispersion, and thermal and dynamic mechanical properties of LDPE/organo-LDH composites. *Express Polymer Letters*, 5(5): 428–448.

Nhlapo, N., Motumi, T., Landman, E., Verryn, S. M. C. & Focke, W. W. (2008). Hydrotalcite: Surfactant-assisted fatty acid intercalation of layered double hydroxides. *J. Mater. Sci.*, 43(3): 1033–1043.

Nyambo, C., Kandare, E., Wang, D. & Wilkie, C. (2008). Flame-retarded polystyrene: Investigating chemical interactions between ammonium polyphosphate and MgAl layered double hydroxide. *Polym. Degrad. Stab.*, 93: 1656–1663.

Nyambo, C., Wang, D. & Wilkie, C. (2009). Will layered double hydroxides give nanocomposites with polar or non-polar polymers? *Polym. Adv. Technol.*, 20: 332–340.

O'Leary, S., O'Hare, D. & Seeley, G. (2002). Delamination of layered double hydroxides in polar monomers: New LDH-acrylate nano composites. *Chem. Comm.*, 14: 1506–1507.

Okada, A. & Usuki, A. (1995). The chemistry of polymer-clay hybrids. *Mater. Sci. Eng. C.*, 3: 109–115.

Peeterbroeck, S., Alexandre, M., Jerome, R. & Dubois, P. (2005). Poly(ethylene-co-vinyl acetate) clay nanocomposites: Effect of clay nature and organic modifiers on morphology, mechanical and thermal properties. *Polym. Degrad. Stab.*, 90: 288–294.

Pradhan, S., Costa, F. R., Wagenknecht, U., Jehnichen, D., Bhowmick, A. K. & Heinrich, G. (2008). Elastomer/LDH nanocomposites: Synthesis and studies on nanoparticle dispersion, mechanical properties and interfacial adhesion. *Eur. Polym. J.*, 44(10): 3122–3132.

Qiu, L., Chen, W. & Qu, B. (2005). Structural characterisation and thermal properties of exfoliated polystyrene/ZnAl layered double hydroxide nanocomposites prepared via solution intercalation, 87: 433–440.

Ramaraj, B. & Yoon, K. (2008). Thermal and physicomechanical properties of ethylene□vinyl acetate copolymer and layered double hydroxide composites. *J. Appl. Polym. Sci.*, 108: 4090–4095.

Ramaraj, B., Nayak, S. & Yoon, K. (2010). Poly(vinyl alcohol) and layered double hydroxide composites: Thermal and mechanical properties. *J. Appl. Polym. Sci.*, 116: 1671–1677.

Ray, S. S. & Okamoto, M. (2003) Polymer/layered silicate nanocomposites: A review from preparation to processing. *Prog. Polym. Sci.*, 28(11):1539–1641.

Riva, A. (2002). Thermal degradation and rheological behaviour of EVA/montmorillonite nanocomposites. *Polym. Degrad. Stab.*, 77(2): 299–304.

Solin, S. A., Hines, D., Yun, S. K., Pinnavaia, T. J. & Thorpe, M. F. (1995). Layer rigidity in 2-D disordered Ni-Al layer double hydroxides. *J. Non-Cryst. Solids*, 182: 212–220.

Utracki, L. A. (2004). *Clay-Containing Polymeric Nanocomposites*, Vol. 1. Shrewsbury, UK: Rapra Technology Ltd, p. 456.

Utracki, L. A., Sepehr, M. & Boccaleri, E. (2007). Synthetic, layered nanoparticles for polymeric nanocomposites (PNCs). *Polym. Adv. Technol.*, 18(1): 1–37.

Vaia, R. & Wagner, H. (2004). Framework for nanocomposites. *Materials Today*, 32–37.

Vaia, R. A. & Giannelis, E. P. (1997). Polymer melt intercalation in organically-modified layered silicates: Model predictions and experiment. *Polymer*, 9297(96): 8000–8009.

Vaysse, C., Guerlou-Demourgues, L., Duguet, E. & Delmas, C. (2003). Acrylate intercalation and in situ polymerization in iron-, cobalt-, or manganese-substituted nickel hydroxides. *Inorg. Chem.*, 42(15): 4559–67.

Verbeek, C. R .J. & Focke, W. W. (2002) Modelling the Young's modulus of plate;et reinforced thermoplastic sheet composites. *Composites Part A*. 33: 1697–1704.

Vieille, L., Moujahid, E. M. &Taviot-gue, C. *et al*. (2004). In situ polymerization of interleaved monomers:a comparative study between hydrotalcite and hydrocalumite host structures. *J. Phys. Chem. Solids*. 65: 385–393.

Wang, B., Zhang, H., Evans, D.G. & Duan, X. (2005). Surface modification of layered double hydroxides and incorporation of hydrophobic organic compounds. *Mater. Chem. Phys.*, 92: 190–196.

Wang, D.-Y., Leuteritz, A., Kutlu, B., Landwehr, M. A. D., Jehnichen, D., Wagenknecht, U. & Heinrich, G. (2011). Preparation and investigation of the combustion behavior of polypropylene/organomodified MgAl-LDH micro-nanocomposite. *J. Alloys Compd.*, 509(8): 3497–3501.

Wang, G., Wang, C. & Chen, C. (2006). The disorderly exfoliated LDHs/PMMA nanocomposites synthesized by in situ bulk polymerization: The effects of LDH-U on thermal and mechanical properties. *J. Phys. Chem. B.*, 91: 2443–2450.

Wang, L., Li, B., Chen, C. & Jia, L. (2010). Structural characterization and related properties of the stearate anions intercalated Ni–Al hydrotalcite-like compound prepared by the microwave crystallization. *J. Alloys Compd.*, 508(2): 426–432.

Ward, I. M. & Hadley, D. W. (1993) *An Introduction to Mechanical Properties of Solid Polymer*s, 1st ed. New York: Wiley.

Whilton, N. T., Vickers, P. J. & Mann, S. (1997). Bioinorganic clays: synthesis and characterization of amino- and polyamino acid intercalated layered double hydroxides. *J. Mater. Chem.*, 7(8): 1623–1629.

Work, W. J., Horie, K., Hess, M. & Stepto, R. F. T. (2004). Definition of terms related to polymer blends, composites, and multiphase polymeric materials (IUPAC Recommendations). *Pure Appl. Chem.*, 11: 1985–2007.

Xu, Z. P & Braterman, P. (2010). Synthesis, structure and morphology of organic layered double hydroxides (LDH) hybrids: Comparison between aliphatic and their oxygenated analogs. *Appl. Clay Sci.*, 48: 235–242.

Zammarano, M., Bellayer, S., Gilman, J. W., Franceschi, M., Beyer, F. L., Harris, R. H. & Meriani, S. (2006). Delamination of organo-modified layered double hydroxide in polamide by melt processing. *Polymer*, 47: 652–662.

Zammarano, M., Franceschi, M., Gilman, J. W. & Meriani, S. (2005). Preparation and flame resistance properties of revolutionary self-extinguishing epoxy nanocomposites based on layered double hydroxides. *Polymer*, 46: 9314–9328.

Zubitur, M. A., Gomez, M. & Cortazar, J. (2009). Structural characterisation and thermal decomposition of layered double hydroxide/poly(p-dioxanone) nanocomposites. *Polym. Degrad. Stab.*, 94: 804–809.

Zuiderduin, W. C. J., Westzaan, C., Huétink, J. & Gaymans, R. J. (2003) Toughening of polypropylene with calcium carbonate particles. *Polymer*, 44: 261–275.